Micro- and Nanorobots meet DNA

Mario Urso[1], Martin Pumera[1,2,3,4*]

[1] Future Energy and Innovation Laboratory, Central European Institute of Technology, Brno University of Technology, Purkyňova 123, 61200 Brno, Czech Republic

[2] Center for Advanced Functional Nanorobots, Department of Inorganic Chemistry, Faculty of Chemical Technology, University of Chemistry and Technology Prague, Technická 5, 166 28 Prague, Czech Republic

[3] Center for Nanorobotics and Machine Intelligence, Department of Chemistry and Biochemistry, Mendel University in Brno, Zemedelska 1, CZ-613 00, Brno, Czech Republic

[4] Department of Medical Research, China Medical University Hospital, China Medical University, No. 91 Hsueh-Shih Road, Taichung, Taiwan

E-mail: martin.pumera@ceitec.vutbr.cz

Abstract. DNA, the well-known molecule that carries the genetic information of almost all forms of life, represents a pivotal element in formulating intelligent micro/nanorobotic systems. DNA-functionalized micro/nanorobots have opened new and exciting opportunities in many research areas due to the synergistic combination of self-propulsion at the micro/nanoscale and the high programmability of DNA interactions. Here, we critically reviewed their designs and applications, which span from the use of DNA as the fuel to

chemotactically power nanorobots toward cancer cells to DNA as the main building block for sophisticated phototactic biorobots, DNA nanodevices to self-monitor microrobots activity status, DNA and RNA sensing, nucleic acids isolation, gene therapy, and water purification. We also share our perspective on future directions of the field, envisioning DNA-mediated reconfigurable assemblies of nanorobotic swarms.

Keywords: nanomotors, micromotors, DNA, RNA, aptamers, oligonucleotides, nucleic acids, motion-based sensing, fluorescence, gene delivery, gene silencing, water remediation

1. Introduction

DNA is the most famous biological molecule, carrying the genetic information for the development and functions of living beings through sequences of nucleotides, adenine (A), thymine (B), cytosine (C), and guanine (G). Functional information encoded in DNA covers the sequence-determined binding of proteins, reactivity to enzymes, catalytic properties, and the recognition of low-molecular-weight substrates or macromolecules.[1] DNA mainly adopts the form of a double-stranded helix through A-T and G-C Watson-Crick base pairing. The helix has a diameter of 2 nm and a long persistence length of 50 nm, making DNA a quite stiff nanoscale polymer.[2] Watson-Crick base pairing is highly specific, reversible, tunable in strength, and programmable. Moreover, DNA is biocompatible and biodegradable, and it can be rapidly synthesized and modified using automated methods. Therefore, it represents the ideal building block for formulating sophisticated structures.[3]

On these bases, DNA nanotechnology was invented in the early 1980s by Seeman and has exponentially grown since then.[4] Indeed, by exclusively using DNA as an engineering material, from simple molecules to complex molecular machines that move or process information at the nanoscale have been realized with customized sizes and shapes, controllable surface chemistry, and dynamic function.[5,6] Different research areas can be identified within this field, among which sensing based on nucleic acids recognition ability, drug delivery to living cells, DNA-mediated self-assembly of colloidal systems, and biocomputing.[7,8]

Micro/nanorobots are at the forefront of the research in materials science and nanotechnology, owing to the synergy between the unique and enhanced physicochemical properties of micro/nanoscale materials with the active motion dimension.[9,10] These smart small-scale robotic systems are designed in such a way to harvest

energy from the surrounding environment and convert it into a powerful propulsive force, similarly to bacteria.[11–13] Their autonomous movement improves their activity, overcoming the limit of passive diffusion, and allows them to reach previously inaccessible locations. At the same time, they are devised to perform intricate tasks, finding application in sensors, medicine, and water purification.[14–17]

In the last decade, DNA and micro/nanorobots came into contact. Consequently, an increasing number of works has been reported, demonstrating how the marriage between these two technologies promises to revolution all research areas. This review presents the most advanced designs and applications of DNA-modified micro/nanorobots (Figure 1). It is worth noting that the micro/nanorobots described here are nano- to microscale structures moving at relatively high speeds, ranging from few to hundreds of $\mu m\ s^{-1}$. These are distinct from DNA molecular machines such as the DNA walkers, which are molecular- to nanoscale structures moving up to tens of $nm\ s^{-1}$ thanks to legs that hybridize and destroy complementary nucleic acids immobilized on a surface.[18] Thus, we recommend a recent and relevant review for those readers interested in DNA molecular machines.[19] Instead, in this work, we focus on the new concepts and prospects resulting from the intersection between DNA and micro/nanorobotics. First, the actuation mechanisms of DNA-modified micro/nanorobots are briefly introduced. Then, innovative DNA-based strategies to power and monitor their propulsion are illustrated. Next, the applications of DNA-modified micro/nanorobots are extensively and critically discussed, including DNA and RNA motion- and fluorescence-based sensing, nucleic acids isolation, gene therapy, and water remediation. Finally, a perspective on future directions of the field is shared, predicting the development of DNA-programmable reconfigurable self-assemblies of nanorobotic swarms as a new class of intelligent, cooperative nanorobots.
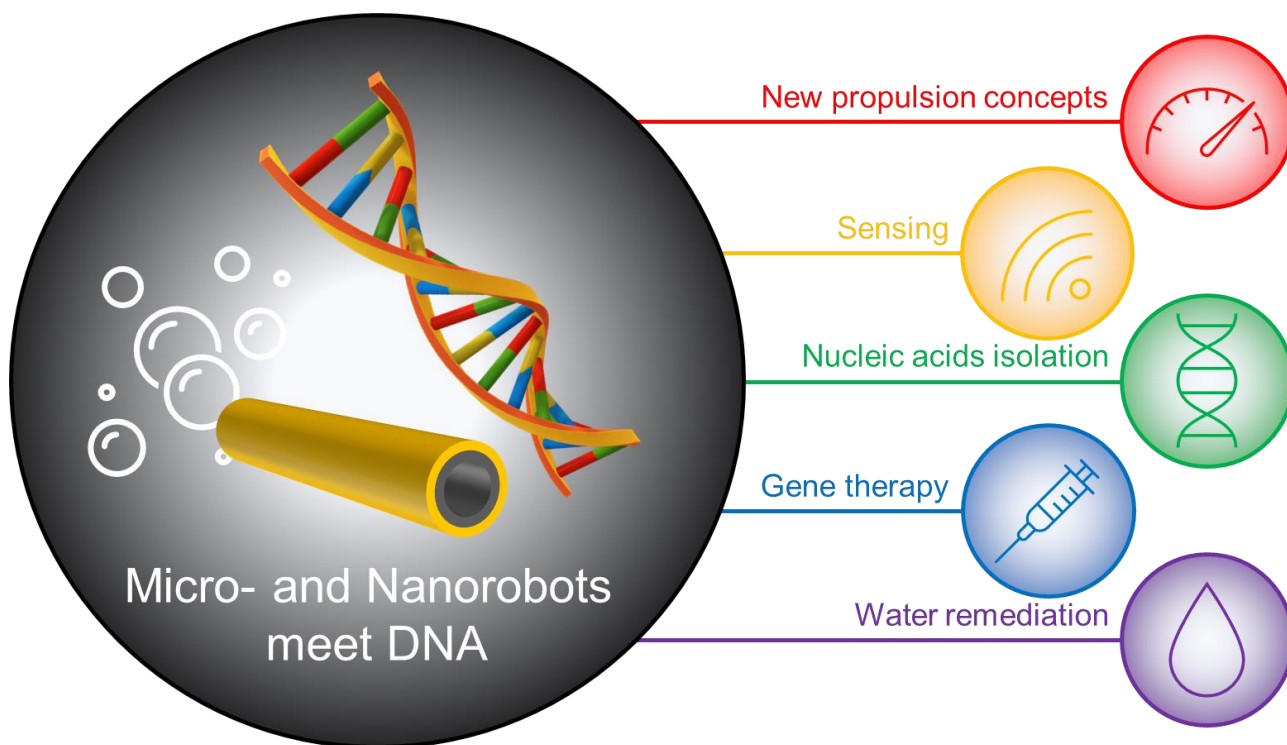
Figure 1. Research directions of DNA-modified micro/nanorobots presented in this review.

2. DNA-modified micro- and nanorobots actuation

Self-propulsion represents the principal requirement for a micro/nanorobot, allowing precise navigation toward the targeted site where desired tasks are performed or accelerating a catalytic or recognition process. This ability can be activated by external energy sources, such as light, acoustic and magnetic fields, or local fuel consumption.[11] Each actuation mode has its *pros* and *cons*. The light-driven motion is primarily attractive for water remediation with photocatalytic semiconductors.[20–22] Enzymatic micro/nanorobots are more appropriate for biomedical applications but limited to human body regions where a specific biomolecule is available.[23] Instead, magnetic manipulation offers high precision in the whole body without fuels.[24] In light of this, it is not surprising that preferential propulsion methods emerged while reviewing the literature on DNA-modified micro/nanorobots, including catalytic, acoustic, and magnetic. This section briefly introduces these motion mechanisms. We believe it can provide helpful information for readers unfamiliar with the field and facilitate the comprehension of the works presented in sections 3 and 4.

The bubble-propelled tubular microrobots are the most reported among DNA-modified micro/nanorobots. For this reason, their fabrication procedure deserves to be shortly introduced. Their peculiar tubular structure is typically obtained by the membrane template-assisted deposition method, as illustrated in Figure 2(a).[25] A

4

commercially available membrane (for example, polycarbonate) serves as the template for depositing an outer functional layer (e.g., Au or various polymers) followed by an inner Pt layer. The depositions are carried out by physical vapor deposition (PVD) processes (magnetron sputtering, electron-beam evaporation, atomic layer deposition) or by electrochemical techniques, which require low-cost apparatus. However, metalization of the membrane, i.e., the coating with a thin metal layer by PVD to improve its conductivity, is necessary for electrodeposition. The membrane's dissolution using an appropriate solvent (for instance, dichloromethane for polycarbonate) releases the microrobots. Figure 2(a) also reports the SEM images of a characteristic tubular microrobot showing the outer functional and inner Pt layers. The advantages of this approach are the high simplicity, reproducibility, and monodispersity of the resulting microrobots. Alternatively, they can be prepared by the strain-assisted rolling of functional nanomembranes on polymers.[26] The propulsion of these rocket-like micromachines originates from the Pt catalyzed decomposition of H_2O_2 fuel into H_2O and O_2 inside the tube. The nucleated O_2 bubbles are continuously ejected from the larger end of the tube, producing a strong propulsion force that pushes it forward, as displayed in Figure 2(a).[27] The presence of low concentrations of surfactants, such as sodium dodecyl sulfate (SDS) and Triton-X, enhances bubble evolution, increasing microrobots speed. The insertion of a ferromagnetic layer (Ni, Fe) between the outer and inner layers unlocks the possibility of magnetic steering and collectability.[23]

The membranes pore size is a key parameter since it governs the dimension of the resultant machines. Therefore, nanoscale robots can be made by choosing a membrane with submicrometer pores. Moreover, tubular or rod/wire-like nanostructures can be achieved by filling the pores through tuning the parameters of the deposition technique. In this way, Au-Pt nanowires can be formed by the consecutive electrodeposition of Au and Pt segments inside nanopores, which propel in H_2O_2 solutions *via* self-electrophoresis, as depicted in Figure 2(b).[28] This mechanism is based on the generation of a gradient of charges, establishing a local electric field that drives the movement of a particle. For Au-Pt microrobots, oxidation of H_2O_2 occurs at the Pt side of the nanowire contemporarily to the reduction of H_2O_2 at the Au side. The excess of protons (H^+) at the Pt side produces an electric field pointing from Pt to Au. This, in turn, leads to the motion of the negatively charged nanorobots with the Pt side forward. It should be noted that the operation of these nanorobots is limited to low-ionic strength media, contrarily to the bubble-propelled tubular microrobots.[29] Again, this nanowire design can comprise magnetic features by introducing a ferromagnetic segment.

Enzymatic micro/nanorobots exploit enzyme-triggered chemical reactions to release the energy stored in the chemical bonds of a substrate (fuel) and translate it into active movement.[30] Catalase is the most used enzyme for the works presented in this review. Like Pt, it decomposes H_2O_2 at one of the highest enzymatic turnover rates (more than one million H_2O_2 molecules per catalase unit). This process leads to bubble-propulsion or self-phoresis.[31] Nevertheless, H_2O_2 toxicity may constitute a problem for biological applications. On the contrary, other enzymes functioning with biocompatible substrates, such as the urease-urea couple, are particularly attractive.[32] In this context, the following section presents the innovative concept of DNA-powered nanorobots. In general, the prerequisite for self-propulsion is to break the symmetry of the system, which can be attained by the asymmetric immobilization of the enzyme on the particle's surface, as shown in Figure 2(c).

Acoustically-propelled nanorobots have been frequently employed for *in vivo* applications (Figure 2(d)).[33] Indeed, the use of ultrasound at sufficiently low amplitudes (MHz frequency range) does not harm biological samples, such as cells and tissues, while driving the movement of nanorobots. This actuation mode is based on the drifting caused by acoustic radiation forces (also called acoustic radiation pressure) exerted on solid objects in a fluid exposed to a sound wave field.[34] Simple ultrasound-powered nanorobots are represented by the Au nanowires fabricated by membrane template-assisted Au electrodeposition, whose surface can be facilely customized with thiolated DNA strands exploiting the strong Au-S covalent bond.

The excellent control over the movement of magnetic micro/nanorobots is particularly promising in biomedical applications.[24] Magnetic actuation requires incorporating a ferromagnetic element in the material's design. The motion is then based on the magneto-phoretic mechanism in magnetic field gradients, i.e., spatially inhomogeneous fields, or the magnetic torque transfer under rotating magnetic fields.[35] The latter can be generated by systems of orthogonal coil pairs, and are characterized by a rotating field vector. Helical structures are particularly attractive among the different magnetic micro/nanorobots. In fact, as depicted in Figure 2(e), they efficiently traduce the rotational movement due to a low-strength rotating magnetic field into a translation movement in a screw-like manner.[34]
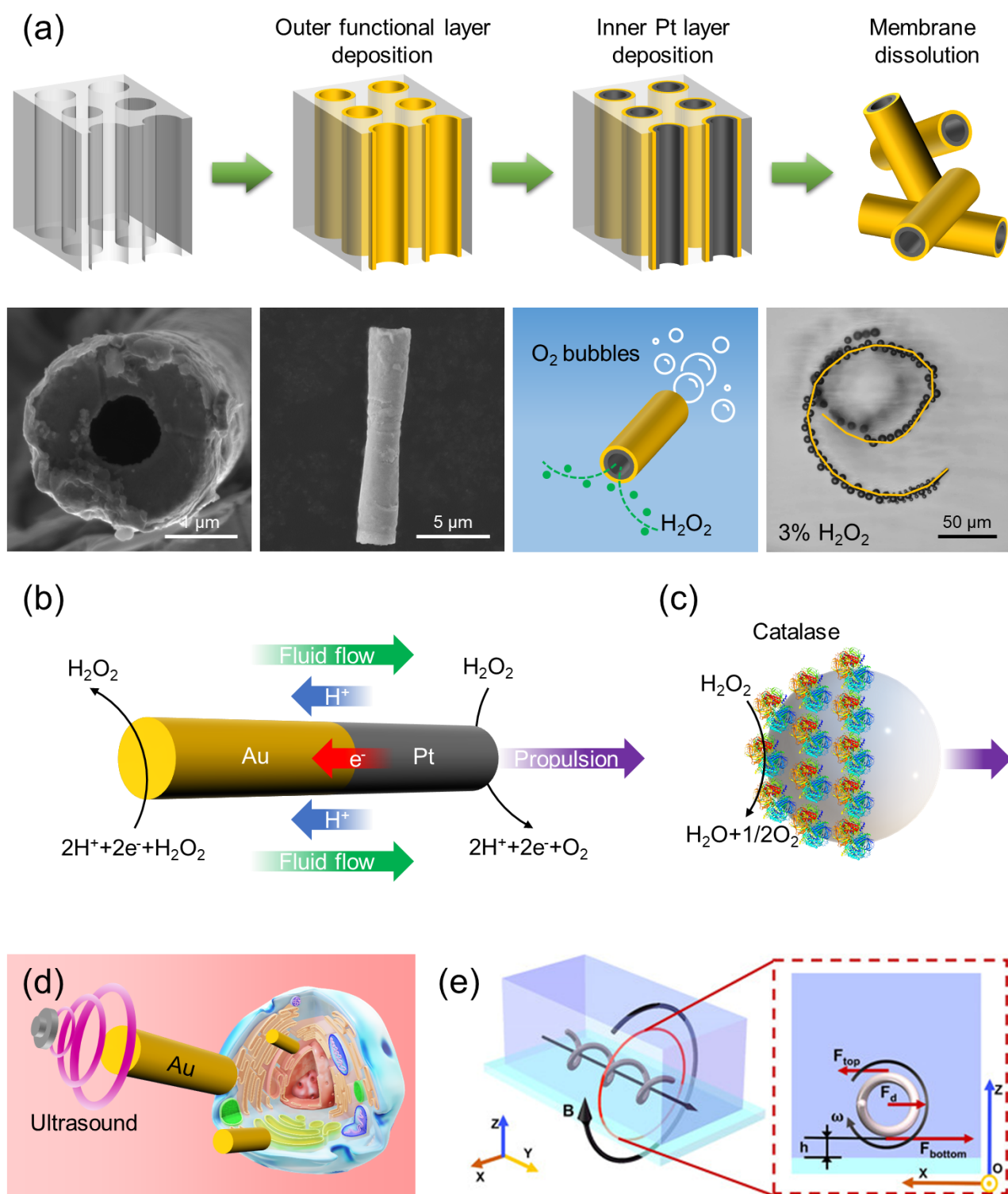
Figure 2. DNA-modified micro/nanorobots actuation modes. (a) Membrane template-assisted deposition method to fabricate bubble-propelled tubular microrobots. SEM images of tubular microrobots showing the outer functional and inner Pt layers. Propulsion mechanism of bubble-propelled tubular microrobots: the inner Pt layer catalyzes the decomposition of H_2O_2, producing O_2 bubbles; continuous ejection of O_2 bubbles pushes the microrobot forward. Time-lapse image showing the trajectory of a tubular microrobot in 3% H_2O_2 and 0.1% SDS after 1 s. Adapted with permission from [25]. Copyright 2021 Wiley. (b) Au-Pt nanowires propulsion mechanism: H_2O_2 is oxidized at the Pt side and reduced at the Au side; the excess of protons (H^+) at the Pt side produces an electric field pointing from Pt to Au, which induces the motion of the negatively charged nanorobots with the Pt side forward. (c) Catalase-modified Janus microrobots propulsion mechanism by the catalyzed decomposition of H_2O_2. (d) Schematic illustration of ultrasound-powered Au nanowires for cell internalization. (e) Magnetic helical micro/nanorobots propulsion mechanism under a rotating magnetic field: the helix's rotation is traduced into a translational movement. Adapted with permission from [34]. Copyright 2020 AIP Publishing.

3. DNA to power and monitor micro- and nanorobots propulsion

This section presents the strategies explored so far to induce the movement of micro/nanorobots through DNA. A unique example of nanorobots equipped with DNA nanodevices to self-monitor their motion status is also described.

Enzymatic micro/nanorobots are generally powered by hydrogen peroxide, glucose, and urea fuels at high concentrations (mM to M levels). Recently, biocompatible nanorobots fueled by ultralow DNA concentrations (nM to μM levels) have been reported.[36] These nanorobots consisted of Janus nanoparticles asymmetrically functionalized with the enzyme DNase, which catalyzes DNA hydrolysis and chemotactically drives their propulsion toward DNA richer regions such as those close to apoptotic tumor cells (Figure 3(a)). Au-poly(acrylic acid) (Au-PAA) Janus nanoparticles were prepared via a multi-step, facile, and scalable synthetic procedure. Then, mesoporous silica ($mSiO_2$) was grown on the PAA side and loaded with rhodamine B (Rh B) as a model drug. Figure 3(b) shows TEM images of the Au-PAA/$mSiO_2$ Janus nanoparticles (~170 nm in size). Next, Au surface was passivated with methoxy-poly-(ethylene glycol)-thiol (mPEG-SH) to improve nanorobots stability. Finally, DNase was immobilized on the exposed PAA chains through the reaction between carboxylic groups of PAA and amino moieties of DNase.

Rh B fluorescence allowed tracking nanorobots. These displayed the typical Brownian motion in the absence of DNA and enhanced diffusion in its presence due to the DNase-induced DNA hydrolyzation. This reaction established an asymmetric product gradient leading to nanorobots movement via diffusiophoresis combined with a thermal effect due to heat generation. Nanorobots speed increased with DNA concentration, from ~6 μm s^{-1} in 0 μM DNA to ~9 μm s^{-1} in 1.036 μM DNA. Their motion was isotropic as for Brownian particles in the absence of apoptotic tumor cells (Figure 3(c)). However, it turned into a directional motion toward apoptotic tumor cells due to the abnormal release of DNA in their surroundings (Figure 3(d)). This behavior, which occurs in nature for some organisms able to direct their movement according to environmental stimuli gradients, is called chemotaxis. In this case, it was positive chemotaxis since nanorobots moved toward the stimulus.

Moreover, the authors explored and demonstrated nanorobots ability to actively seek tumor sites. Normal 3T3 cells and tumor 4T1 cells were placed into two reservoirs of a Y-shaped microfluidic channel (Figure

3(e)). Apoptosis of 4T1 cells was induced before injecting nanorobots on the third reservoir. By monitoring the fluorescence intensity in the three reservoirs, it was shown that nanorobots preferentially accumulate in the 4T1 cells reservoir (Figure 3(f)). Instead, a control experiment using Janus nanoparticles without DNase indicated the uniform distribution of the nanoparticles in the two reservoirs with the cells. These findings prove the potential of such a new class of DNA-powered nanorobots to target, approach, and release drugs in the diseased site, which is highly demanded for tumor diagnosis and therapy.
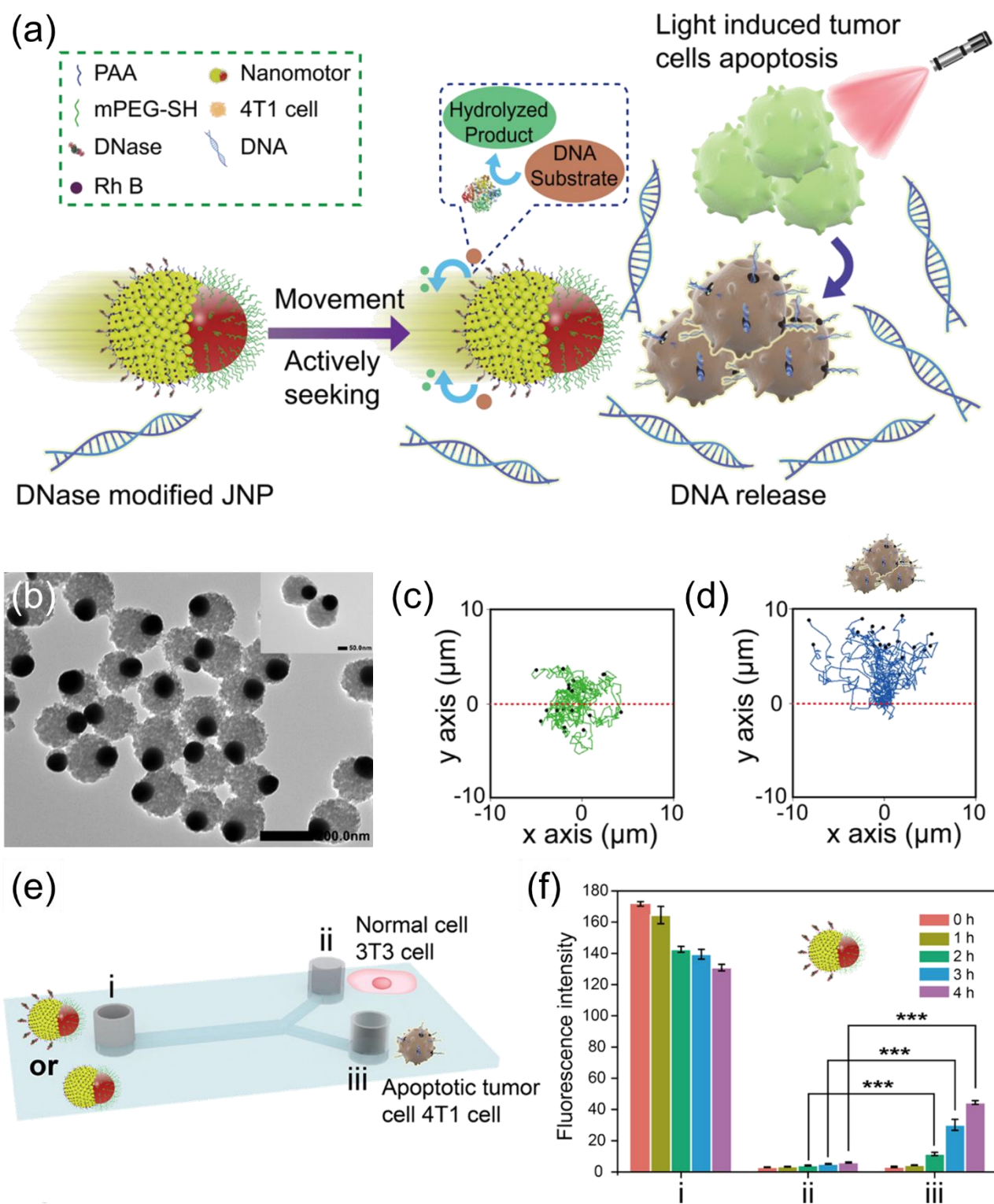
Figure 3. DNA-powered chemotactic nanorobots. (a) Schematic illustration of the motion mechanism of DNase-modified RhB-loaded PEG-Au-PAA/mSiO$_2$ Janus nanorobots by catalyzed DNA hydrolyzation and chemotaxis toward the DNA-rich region around apoptotic tumor cells. (b) TEM images of Au-PAA/mSiO$_2$ Janus nanoparticles. Scale bar is 200 nm (50 nm for the inset). (c) Trajectories of 20 nanorobots exhibiting isotropic motion in the absence of apoptotic tumor cells and (d) directional motion toward apoptotic tumor cells. (e) Chemotaxis experiment in a Y-shaped microchannel with nanorobots placed in reservoir i, normal 3T3 cells in reservoir ii, and apoptotic tumor 4T1 cells in reservoir iii. (f) Fluorescence intensity in the three reservoirs as a function of time, indicating the progressive and preferential accumulation of nanorobots in the reservoir with apoptotic tumor 4T1 cells. Adapted with permission from [36]. Copyright 2021 American Chemical Society.

DNA can be used not only as a fuel but also as the main component to build light-driven micro/nanorobots.[37] This innovative concept is based on the asymmetric growth of peptide nanofibers on nucleospheres under UV-light irradiation. Nucleospheres are submicrometer to micrometer-sized self-assembled DNA spheres obtained through the thermal annealing of three different single-stranded DNA (ssDNA) sequences with self-complementary sticky ends. These DNA microparticles possess the advantage of easy modification with functional molecules, which is crucial for the proposed propulsion strategy. By using a biotinylated ssDNA, biotin-containing nucleospheres were synthesized and modified with streptavidin and biotin-dT_{20} ssDNA (Figure 4(a)). Next, a peptide-DNA conjugate, made of FKFEFKFE nanofiber-forming-unit and dA_{20} ssDNA linked by a photocleavable amino acid, was immobilized on the nucleospheres using the biotin-streptavidin interaction and DNA hybridization (Figure 4(b)). Confocal laser scanning microscopy (CLSM) images of nucleospheres exposed to UV-light irradiation for 3 min (Figure 4(c)) showed how the release of the peptide unit on the irradiated side of the nucleosphere resulted in the asymmetric formation of peptide nanofibers.

In the dark, these microrobots exhibited the characteristic isotropic trajectories of Brownian particles (Figure 4(d)). Under UV-light irradiation, they manifested a directional motion against the light source (Figure 4(e)), called negative phototaxis. This behavior was due to the force generation caused by peptide nanofibers growth and the Marangoni effect owing to the surface tension gradient between the two sides of the microrobots. The speed was higher in the presence of an excess amount of peptide-DNA conjugate in solution, which assisted peptide nanofiber progression, reaching a value of ~5 μm min^{-1}. Furthermore, the propulsion persisted after turning off the UV-light source. This peculiar design serves as the inspiration for bio-microrobots mimicking natural phototactic systems. Nevertheless, microrobots speed is significantly lower than the aforementioned DNA-fueled nanorobots.
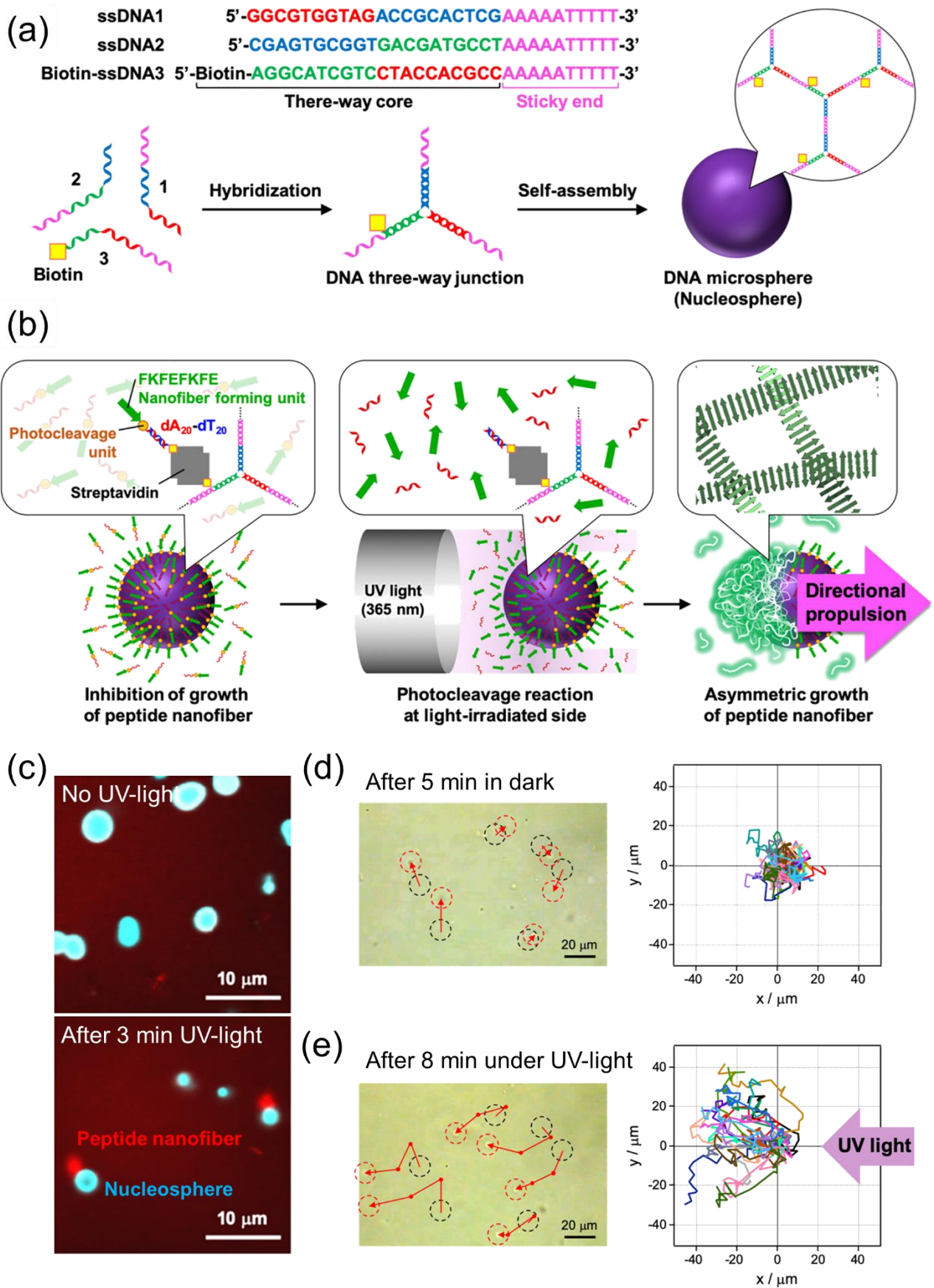
Figure 4. Light-driven phototactic DNA microrobots. (a) Schematic illustration of nucleospheres preparation and (b) phototaxis due to the UV-light-induced asymmetric growth of peptide nanofibers. (c) CLSM images of nucleosphere before and after 3 min under UV-light irradiation. Nucleospheres were stained with DAPI (cyan), the nanofiber forming unit was labeled with TMR (red). (c) Time-

lapse images and trajectories of 20 microrobots showing isotropic Brownian motion after 5 min in the dark and (d) directional motion against the light source (negative phototaxis) after 8 min under UV-light irradiation. Adapted with permission from [37]. Copyright 2021 American Chemical Society.

DNA nanodevices responding to various biological and chemical stimuli hold great promise for the intelligentization of micro/nanorobots. In this regard, it has been demonstrated that pH-sensitive DNA nanoswitches allow real-time monitoring of microrobots activity status (for instance, the speed).[38] Figure 5(a) illustrates the fabrication of urea-powered microrobots. Briefly, a SiO_2 layer was grown on polystyrene (PS) beads using APTES and TEOS precursors. The PS core was removed by DMF, leaving hollow SiO_2 microcapsules with a size of ~2 μm (Figure 5(b)). These were functionalized with urease and DNA nanoswitches. Urease was included to induce microrobots motion via the catalyzed decomposition of urea into ammonia (NH_3) and carbon dioxide (CO_2) (Figure 5(c)). The nanoswitch, depicted in Figure 5(d), consisted of a triplex DNA structure that could be opened or closed depending on the surrounding pH owing to pH-insensitive Watson-Crick interactions and pH-sensitive Hoogsteen interactions. Cyanine-3 (Cy3) fluorophore was conjugated to the duplex DNA, while cyanine-5 (Cy5) fluorophore was conjugated to the triplex-forming DNA strand to visualize the open/close grade of the nanoswitch. At acidic pH values (pH<6), the nanoswitch was closed, and the proximity between Cy3 and Cy5 resulted in Förster Resonance Energy Transfer (FRET) emission. At higher pH values (pH>6), the nanoswitch opened, and FRET emission was hindered. At the same time, a stronger Cy3 emission was detected, diminishing the FRET/Cy3 ratio.

This system permitted the visualization of microrobots status. In fact, by introducing urea, microrobots were initially propelled at a speed of ~6 μm s^{-1} due to urea decomposition by urease. A FRET/Cy3 ratio of ~2 was registered in this stage. Contemporarily, the produced ammonia gradually increased the local pH around the microrobots, closing the nanoswitches and reducing FRET emission. Figure 5(e) shows the FRET/Cy3 ratio over time. The same trend was observed for microrobots speed (Figure 5(f)). This behavior was due to the decreasing urease activity (Figure 5(g)), which in turn lowered microrobots speed and FRET/Cy3 ratio. Such correlation represents a smart approach for microrobots speed imaging during their operation. Besides, it may be applied for evaluating intracellular and intra-tissue pH values.
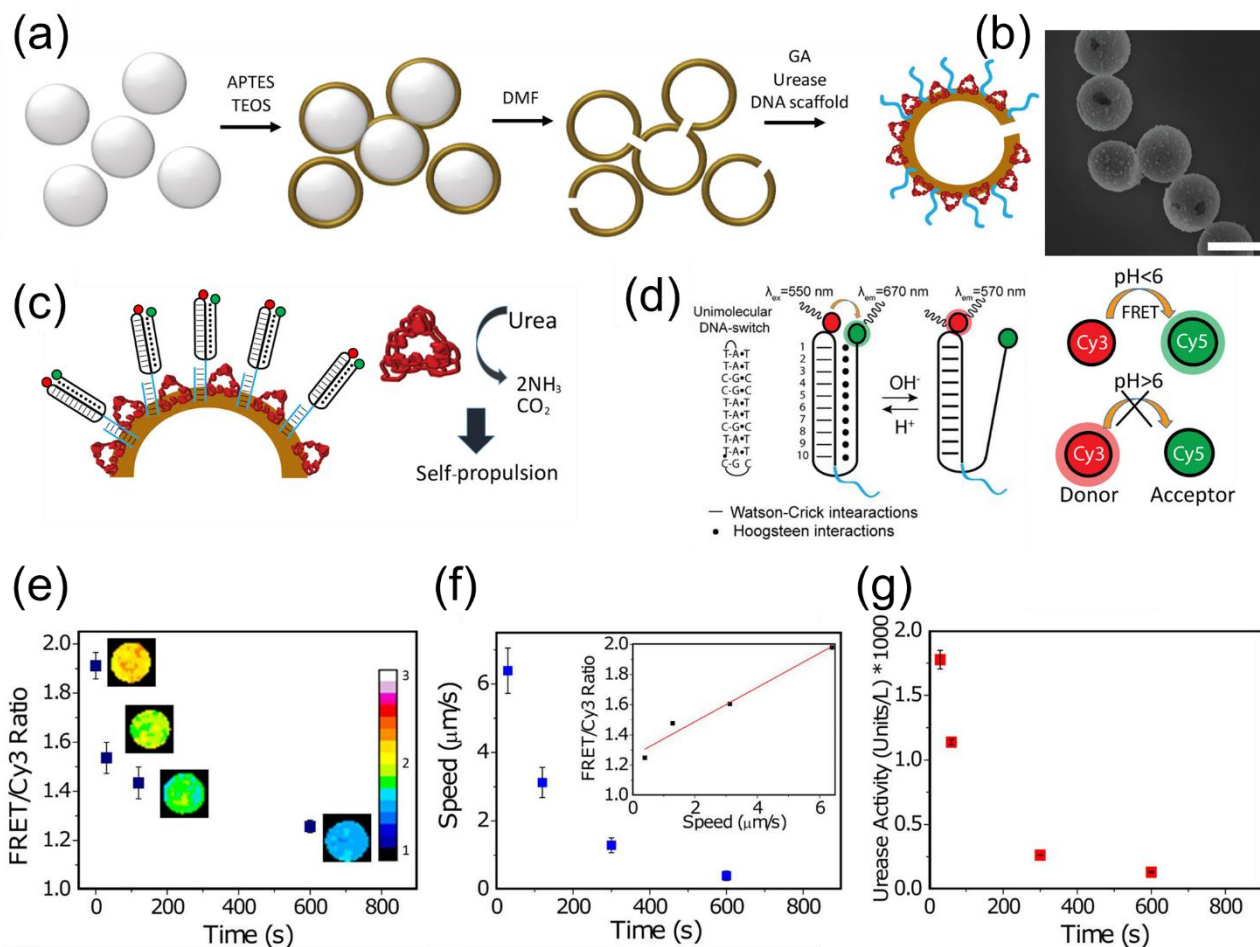
Figure 5. Self-sensing enzyme-powered DNA microrobots. (a) Schematic illustration of microrobots fabrication. (b) SEM image of hollow SiO_2 microcapsules. Scale bar is 2 μm. (c) Schematic diagram of microrobots propulsion mechanism and (d) DNA nanoswitch operation at acidic and basic pH values. (e) FRET/Cy3 ratio of microrobots incubated with 100 mM urea at different times. CLSM images of a microrobot allowing the FRET/Cy3 ratio visualization are reported. (f) Microrobots speed at different times. The inset shows the correlation between speed and FRET/Cy3 ratio. (g) Microrobots enzymatic activity at different times. Adapted with permission from [38]. Copyright 2019 American Chemical Society.

4. Applications of DNA-modified micro- and nanorobots

This section describes the most relevant contributions of DNA-modified micro/nanorobots in various application fields, ranging from DNA and RNA detection to the isolation of nucleic acids, gene therapy, and water purification.

4.1. DNA and RNA sensing

Traditional methods for DNA and RNA detection, including the highly sensitive and selective polymerase chain reaction (PCR), are expensive, time-consuming, and require laboratory instruments operated by trained personnel due to their complex operational protocols.[39] By contrast, the rapid diffusion of coronavirus disease

14

2019 (COVID-19) has demonstrated how crucial the timely identification and management of infectious diseases is. Recently, DNA-modified micro/nanorobots have opened new opportunities in this context. Different approaches can be identified according to the sensing mechanism: (1) motion-based sensors translate probe-target hybridization events into appreciable differences in micro/nanorobots motion or speed; (2) fluorescent recovery-based sensors exploit micro/nanorobots active movement to accelerate the hybridization, producing a detectable optical signal; (3) motion- and fluorescence-based sensors, where microrobots fluorescence intensity and speed vary as a result of the hybridization. The most significant examples related to these three categories are presented below.

4.1.1.   Motion-based sensing

Wang's research group introduced the concept of motion-based sensing for the first time.[40] This consists of using an optical microscope to track changes of micro/nanorobots speed due to the presence of a target analyte. After proving that trace levels of Ag^+ ions enhanced the speed of catalytic Au-Pt nanowires in H_2O_2, they extended the methodology for the transduction of DNA hybridization.[41] The sensor's operation principle is schematically illustrated in Figure 6(a). A gold electrode functionalized with a thiolated ssDNA probe was used to capture Ag nanoparticles-tagged ssDNA target, forming a dsDNA. Upon exposure to H_2O_2, Ag nanoparticles quickly dissolved, releasing Ag^+ ions. The Ag^+ ions-rich H_2O_2 solution was employed to power fresh Au-Ni-Au-Pt nanowires prepared by membrane template-assisted electrodeposition, which moved *via* the self-electrophoretic mechanism represented in Figure 2(b). By incorporating a ferromagnetic Ni segment, linear trajectories were obtained under a magnetic field, allowing a straightforward comparison between tracks length at a fixed time interval for different amounts of DNA target. As expected, nanorobots track length in 10% H_2O_2 increased with DNA target concentration. A limit of detection (LoD) of 40 amol and $7x10^3$ CFU μL^{-1} was measured for synthetic DNA target and 16S rRNA, released from *E. coli* pathogenic bacteria. The sensor exhibited high specificity against a variety of interferents and reproducible response.

Later on, Nguyen and Minteer presented the "signal on" motion-based DNA sensing.[42] Figure 6(b) illustrates the working principle of the sensor. The inner Au layer of poly(3,4-ethylenedioxythiophene)/Au (PEDOT/Au) tubular microrobots, fabricated by membrane template-assisted electrodeposition, and Pt nanoparticles were modified with two ssDNA sequences, which were partially complementary to an ssDNA

target. Without the target, microrobots self-propulsion in H_2O_2 was not observed. Instead, it linked the Pt nanoparticles to microrobots inner layer when present. Hence, microrobots bubble-propulsion in H_2O_2 was activated, likewise tubular microrobots with a compact Pt layer (Figure 2(a)). A non-complementary sequence did not trigger their motion, suggesting an excellent selectivity. However, this sensor lacked sensitivity since the speed values for 1 and 20 pmol DNA target were relatively similar (157 and 222 μm s^{-1} in 5% H_2O_2, respectively). Of note, compared to the previously described electrocatalytic nanowires, bubble-propelled microrobots allow operation in high-ionic strength solutions.

Wu and coworkers reported a different motion-based sensing approach, inducing a decrease of microrobots speed rather than an increase.[43–45] For this purpose, the authors prepared jellyfish-like Au/Ag/Ni/Au shells (20 μm in size) by successive sputtering deposition of metals on sacrificial SiO$_2$ microspheres (Figure 6(c)). Before SiO$_2$ etching, the outer Au surface was blocked with 6-mercapto-1-hexanol (MCH). In this way, after SiO$_2$ etching, the shell's concave surface was modified with a DNA probe sandwich ("sensing unit") and several catalase layers ("power unit") by cyclic alternate hybridization assembly. By doing so, the shells displayed bubble-propulsion even in low H_2O_2 concentrations (~25 μm s^{-1} in 0.25 H_2O_2). Then, the DNA detection was based on the release of the power unit due to the hybridization between the sensing unit and DNA target, causing the diminution of microrobots speed. An LoD of 10 nM was obtained with this method.

A reliable, affordable, and compact motion-based sensor for HIV-1 infection has also been presented.[46] This integrated loop-mediated isothermal amplification (LAMP) reaction, DNA-modified catalytic microrobots, and cellphone-based optical sensing to record and track microrobots motion (Figure 6(d)). In particular, microrobots were made by asymmetrically coating polystyrene beads (6 μm in size) with Pt nanoparticles (4 nm) and ssDNA probe-modified Au nanoparticles (150 nm). Upon amplification of HIV-1 RNA by LAMP reaction, the microrobots captured the resulting amplicons. As a consequence, a large DNA tail was formed, obstructing microrobots movement in H_2O_2 and, thus, decreasing their speed. This stratagem enabled the detection of HIV-1 at concentrations lower than the clinically relevant threshold of 1000 virus particles mL^{-1} and the discrimination between positive and negative patients. The excellent sensitivity, selectivity, stability, rapidity (<1 h), and low cost (<5 $) of the proposed sensor promise timely management of other infectious diseases in the future.
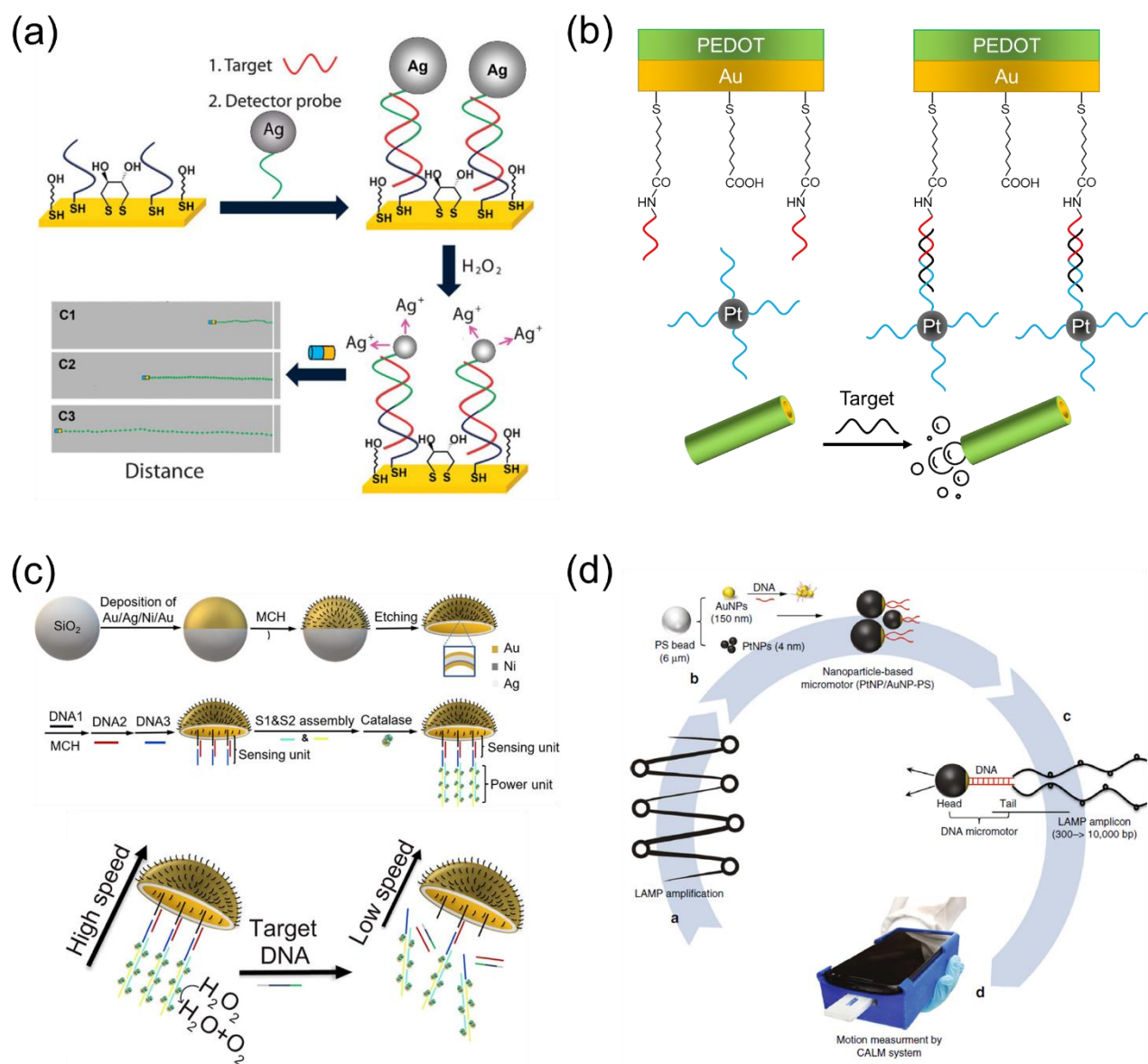
Figure 6. Motion-based DNA sensing strategies. (a) A DNA-modified Au electrode captures an Ag nanoparticles-tagged DNA target. Ag nanoparticles dissolution in H_2O_2 causes the release of Ag^+ ions. This solution is used to fuel electrocatalytic Au-Ni-Au-Pt nanorobots along linear trajectories under magnetic alignment. Straight-line distance signals for increasing DNA target concentrations (C1<C2<C3) are visualized by optical microscopy. Adapted with permission from [41]. Copyright 2010 Springer Nature. (b) The inner surface of PEDOT/Au tubular microrobots and Pt nanoparticles are functionalized with non-complementary DNA sequences. The latter are partially complementary to a DNA target, which, by connecting the Pt nanoparticles to microrobots, triggers their bubble-propulsion in H_2O_2. (c) Jellyfish-like Au/Ag/Ni/Au shells, comprising a DNA probe sandwich ("sensing unit") and several catalase layers ("power unit") prepared by cyclic alternate hybridization DNA assembly, detect a target DNA *via* the hybridization-induced release of the power unit, which causes a decrease of microrobots bubble-propulsion speed in H_2O_2. Adapted with permission from [45]. Copyright 2019 American Chemical Society. (d) HIV-1 motion-based detection using a cellphone system: LAMP reaction amplifies the HIV-1 RNA; DNA-modified catalytic microrobots, consisting of polystyrene microbeads coated by Pt and DNA-modified Au nanoparticles, capture the resulting amplicons; the formed DNA tail decelerates microrobots catalytic propulsion in H_2O_2; a cellphone system measures variations of microrobots speed, allowing to sense HIV-1 at the clinically relevant threshold of 1000 virus particles mL^{-1}. Reproduced with permission from [46]. Copyright 2018 Springer Nature.

4.1.2. Fluorescence recovery-based sensing

Various micro/nanorobots, differing for the material's design or actuation mechanism, have demonstrated the fluorescence detection of cancer biomarkers in a rapid, sensitive, and specific manner. Among the targeted cancer biomarkers is microRNA 21 (miRNA-21), a small RNA highly overexpressed in solid tumors, such as those of brain, head and neck, esophagus, breast, lung, stomach, pancreas, colon, and prostate.[47] Consequently, several works have been focused on miRNA-21 sensing.

First, Wang et al. reported acoustically powered nanorobots for real-time detection of miRNA-21 in single cells.[48] Au nanowires (~300 nm in diameter, 4 μm in length) were fabricated by membrane template-assisted electrodeposition and further modified with a SAM of cysteamine to immobilize graphene oxide (GO) sheets covalently. Then, nanorobots surface was functionalized with a fluorescein amidine (FAM)-labeled ssDNA probe. Figure 7(a) shows the miRNA-21 detection strategy, based on the: (i) FRET quenching of the dye's fluorescence signal caused by the π- π interaction between GO and FAM-labeled ssDNA; (ii) fluorescence recovery as a result of the release and hybridization of FAM-labeled ssDNA with the miRNA-21 target. The intracellular detection of endogenous miRNA-21 was investigated using the breast cancer cell line MCF-7. The nanorobots showed fast internalization and effective movement inside the cells under the application of ultrasound (6 V, 2.66 MHz), which accelerated the hybridization process leading to a quick "OFF-ON" switching of the fluorescence in single MCF-7 cells within 5 min incubation. The method's selectivity was confirmed by a control experiment with HeLa cells, which are characterized by a lower expression of miRNA-21 compared to MCF-7. Indeed, the fluorescence intensity of MCF-7 was 44 times higher than HeLa cells after the treatment with nanorobots.

Subsequently, the same nanorobots were employed to detect human papillomavirus (HPV)-associated head and neck cancer and breast cancer. In the first case, the FAM-labeled ssDNA probe was complementary to the HPV16 E6 mRNA target. After 15 min incubation under ultrasound, nanorobots allowed the successful discrimination between HPV-negative and HPV-positive human oropharyngeal cancer (OPC) cells *via* the fluorescence-recovery mechanism.[49] In the second case, nanorobots were modified with a FAM-labeled DNA aptamer which allowed the detection of the overexpressed amplified in breast cancer 1 (AIB1) protein in MCF-7 cells.[50]

Bubble-propelled tubular microrobots have been used for the "OFF-ON" fluorescence detection of Reprimo RPRM), a gastric cancer biomarker.[51] These microrobots were prepared by membrane template-assisted

deposition through the electrochemical reduction of GO (erGO), followed by the electrodeposition of a Pt layer and the modification with a FAM-labeled RPRM probe. Microrobots propulsion in a solution of 1.5% H_2O_2 and 5 μM RPRM target produced a strong fluorescence signal within 2 min, which was six times higher than the one registered for static microrobots. It is worth mentioning that similar aptamer-modified rGO/Pt tubular microrobots have also been applied to detect different toxins through the same mechanism.[52,53]

The 2D layered material molybdenum disulfide (MoS_2) can replace the role of GO in the fluorescence recovery-based detection of miRNA-21 and proteins.[54] Tubular microrobots were created by membrane template-assisted electrodeposition of MoS_2 and Pt. Microrobots exhibited a high speed of 370 μm s^{-1} in 1% H_2O_2, which was attributed to the granular morphology of the Pt layer. Analogously to GO, MoS_2 quenched the FAM-labeled ssDNA probe's fluorescence, enabling the "OFF-ON" fluorescence detection of miRNA-21 within 5 min in 1% H_2O_2. The same microrobot was used to sense thrombin through a fluorescein isothiocyanate- (FITC) labeled DNA aptamer probe.

Li and coworkers presented the capture-induced ratiometric fluorescence detection of circulating tumor cells (CTCs) by self-motile microrobots (Figure 7(b)).[55] Despite not being strictly related to DNA or RNA sensing, this work provides an original strategy that can be easily extended to DNA and RNA targets. Nonetheless, the rapid detection of CTCs is crucial since the separation of these tumor cells from primary mass indicates cancer progression. With this aim, rod-like polymer-based microrobots were fabricated by the cryo-cutting of Janus fibers synthesized by electrospinning. The two sides of the microrobots were functionalized with catalase and TLS11a aptamers, respectively: the former provided the self-propulsion ability through the catalyzed H_2O_2 decomposition, the latter ensured the specific binding of CTCs. Afterward, aptamers were labeled with tetraphenylethylene (TPE) and FITC through base-pair interactions. TPE aggregation-induced emission (AIE) and FITC aggregation-caused quenching (ACQ) effects resulted in blue fluorescence emission. Microrobots movement accelerated the capture of CTCs, inducing the release of TPE and FITC in the solution. Consequently, TPE AIE diminished, while FITC green fluorescence was reestablished. This ratiometric fluorescence signaling allowed CTCs detection with a low detection limit of 25 cells mL^{-1} within 1 min exposure to microrobots.
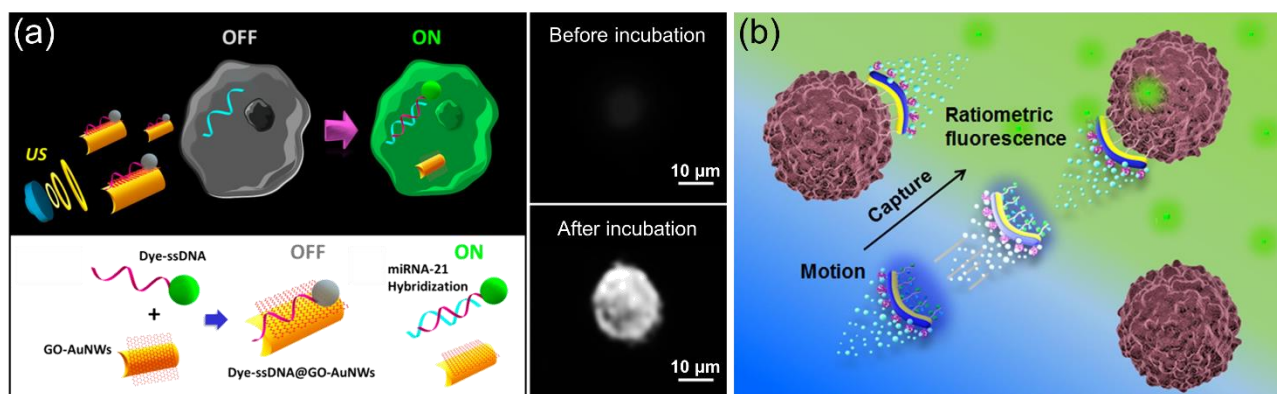
Figure 7. Fluorescence recovery-based sensing strategies. (a) Single-cell miRNA-21 "OFF-ON" fluorescence detection by ultrasound-powered nanorobots: the surface of graphene oxide (GO)/Au nanowires is modified by a dye-labeled ssDNA probe; GO quenches the dye's fluorescence; the latter is recovered due to the release of the ssDNA probe upon hybridization with the miRNA-21 target. Fluorescence microscopy images of an MCF-7 cell before and after 20 min incubation with nanorobots under an ultrasound field (6 V, 2.66 MHz) demonstrate intracellular miRNA detection. Adapted with permission from [48]. Copyright 2015 American Chemical Society. (b) Ratiometric fluorescence detection of circulating tumor cells (CTCs) by catalase-grafted polymer-based Janus microrobots. The binding between TPE and FITC fluorophores with aptamers on microrobots surface resulted in the aggregation-caused quenching (ACQ) effect of FITC and aggregation-induced emission (AIE) of TPE, leading to blue fluorescence emission. CTCs capture caused the release of the fluorophores so that TPE fluorescence was weakened while that of FITC was restored to emit green fluorescence. Reproduced with permission from [55]. Copyright 2020 Elsevier.

4.1.3. Motion- and fluorescence-based detection

Oksuz's research group proposed dual motion- and fluorescence-based detection of miRNA-21 using self-propelled microrobots.[56] Tungsten trioxide (W_5O_{14}) microwires (~100 nm in diameter, ~10 μm in length) were synthesized by chemical vapor transport (CVT) reaction. PEDOT was polymerized on their surface, followed by the sputtering deposition of a Pt layer. Unlike the previously mentioned approaches, an unlabeled ssDNA probe was immobilized on microrobots surface. On the contrary, a FAM-labeled miRNA-21 target was used. In this way, by exposing the microrobots to 100 nM miRNA-21 in 3% H_2O_2, a remarkable increase of their fluorescence intensity was recorded within 15 min, indicating the successful hybridization between probe and target. At the same time, a notable decline of microrobots speed was noted, which changed from 420 to 78 μm s^{-1}. This behavior was explained by the complete blocking of microrobots surface due to the dsDNA formation. W_5O_{14}/Pt microrobots were tested as a control, showing a lower sensitivity. In fact, PEDOT's larger surface area could accommodate more probe sequences, producing larger fluorescence and speed variations. A linear response was observed over the wide range of 1-100 nM miRNA-21 for both the fluorescence and speed signaling modes, from which low LoD values of 28 pM and 21 pM were calculated, respectively.

The motion and fluorescence-based detection of miRNA-21 was also studied for Au/PEDOT/Pt tubular microrobots (2 μm in diameter, ~12 μm in length), fabricated by membrane template-assisted

electrodeposition.[57] In this case, microrobots surface was modified with a FAM-labeled ssDNA probe through hydrophobic and van der Waals interactions. The fluorescence intensity and speed of the microrobots decreased after 5 min incubation with miRNA target due to the occurred hybridization. Of note, Au/PEDOT/Pt microrobots speed (140 μm s^{-1}) was lower than PEDOT/W$_5$O$_{14}$/Pt despite the higher amount of H$_2$O$_2$ (10%) required for their motion. Additionally, a worse LoD of 0.34 nM was attained. Still, the authors showed microrobots antiproliferative effect against breast cancer cells.

The application of surface acoustic waves (SAW) was demonstrated to be an effective strategy to lower the miRNA-21 LoD by removing the unbound ssDNA probe from microrobots surface.[58] Tubular Au/Pt microrobots (1.5-2 μm in diameter, ~10 μm in length) were prepared by membrane template-assisted electrodeposition and functionalized with a FAM-labeled ssDNA probe. Under the SAW, microrobots bubble-propulsion speed in 1% H$_2$O$_2$ increased from ~30 to 50 μm s^{-1}, while the lowered fluorescence intensity confirmed the release of the unbound probe. The beneficial effect of SAW on miRNA-21 response and, thus, LoD were evident since it decreased from 0.41 nM to 0.19 nM for the fluorescence signaling mode.

To avoid using H$_2$O$_2$, the same research group proposed miRNA-21 sensing by magnetically and acoustically powered Au-Ni nanorobots.[59] Au nanowires (200 nm in diameter, 3 μm in length) were fabricated by membrane template-assisted electrodeposition and subsequently coated by a Ni layer through sputtering technique. This design enabled nanorobots dual magnetic and acoustic actuation. Nanorobots displayed a speed of 21.5 μm s^{-1} under a constant magnetic field (22 mT, 20 Hz), which further raised up to 120 μm s^{-1} by the simultaneous application of an acoustic field (3 dBm). As in the previous examples, nanorobots surface was modified with the FAM-labeled ssDNA probe. The hybridization with the miRNA-21 target (0.01-100 nM) significantly quenched nanorobots fluorescence intensity and speed, resulting in ultra-low detection limit values (2.9 and 1.6 pM, respectively) compared to catalytic microrobots. In addition, the *on-site* delivery of doxorubicin (DOX) to breast cancer cells was also investigated, exploiting the high precision of magnetic actuation.

Independently from the sensing mechanism, all examples presented above were based on the functionalization of micro/nanorobots surface with an ssDNA probe for binding a DNA or RNA target. Therefore, their use was limited to the specific target. However, a recent work introduced non-functionalized micro/nanorobots as generic cargo carriers to perform dynamic loading, transport, and release of functionalized

beads.[60] In this way, the same micro/nanorobot can be reused for different targets or detect them at the same time as long as adequately functionalized beads are carried.

4.2. Nucleic acids isolation

Nucleic acids isolation is critical for many biomedical and diagnostic applications. However, current methods at the macroscale are unsuitable for microscale devices. Micro/nanorobots autonomous motion represents a valid solution to this problem. Nucleic acids capture, transport, and delivery by DNA-modified micro/nanorobots rely on the intrinsic specificity of DNA base pairing, allowing to selectively pick up and transport a targeted sequence by immobilizing its complementary on micro/nanorobots surface.

Wang's research group demonstrated the rapid extraction of nucleic acids from raw biological samples using DNA-modified self-propelled microrobots.[61] Pt tubular microrobots were prepared by the strain-assisted rolling of functional nanomembranes on polymers,[26] covered with Au by electron beam evaporation, and functionalized with an ssDNA probe sequence. A fluorophore-labeled ssDNA target was used. Microrobots bubble-propulsion in H_2O_2 resulted in a 13-fold enhancement in the hybridization efficiency compared to static ones. This result was attributed to the generation of fluid vortexes that promoted mass transfer. The lower the sample volume, the stronger the local mixing effect produced. The authors also demonstrated microrobots movement in untreated complex biological samples (plasma, urine, saliva) to capture the target, which was further transported to a "clean" zone where post-processing analyses (for instance, sensing) could be, in principle, conducted (Figure 8(a)).

Besides the capture and transport, achieving the controlled release of the target is essential for post-treatments. Aptamer-functionalized Au/Ni/Pt tubular microrobots have been employed to reach this goal.[62] Microrobots surface was modified with a mixed binding aptamer (MBA) containing both thrombin and adenosine triphosphate (ATP) aptamers via DNA hybridization. While the first aptamer ensured selective isolation and transport of thrombin, the second allowed the release of the MAB-thrombin complex upon swimming in an ATP solution (Figure 8(b)). Such a capture-transport-release approach holds great potential for diverse diagnostic applications.

Similarly, bubble-propelled aptamer-modified Au/Ni/MnO$_2$-polyethyleneimine (Au/Ni/MnO$_2$-PEI) nanorobots were used to collect human promyelocytic leukemia cells (HL-60) in human serum.[63] After

performing the capture, nanorobots were transferred into a second chamber where HL-60 cells were released in the presence of a nucleotide sequence complementary to the aptamer. Further detection of the released HL-60 cells was carried out using an aptamer-modified electrode by electrochemical impedance spectroscopy (EIS) technique, attaining a low detection limit of 250 cells mL^{-1}.

Surface charge-reversible microrobots enabled the controlled extraction and release of nucleic acids through a different mechanism (Figure 8(c)).[64] Tubular microrobots (1-2 μm in diameter, ~10.5 μm in length, ~150 nm in wall thickness), consisting of a ferromagnetic Ni layer embedded in an inner Pt layer and an outer cationic PEI layer, were prepared by membrane template-assisted electrodeposition and carbodiimide chemistry. This design resulted in high-speed bubble-propelled microrobots (~500 μm s^{-1} in 4% H$_2$O$_2$) harboring magnetic properties and pH-dependent surface charge. In acidic solution (pH 4), microrobots positively charged surface allowed capturing FITC-labeled negatively charged nucleic acids by electrostatic attraction with >95% efficiency. After being magnetically transferred to a basic solution (pH 11), microrobots surface turned negative, causing the release of captured nucleic acids with 80% efficiency. Microrobots excellent reusability, selectivity against proteins, and the possibility of guidance in microfluidic channels using an external magnetic field make them particularly attractive for microscale gene isolation.
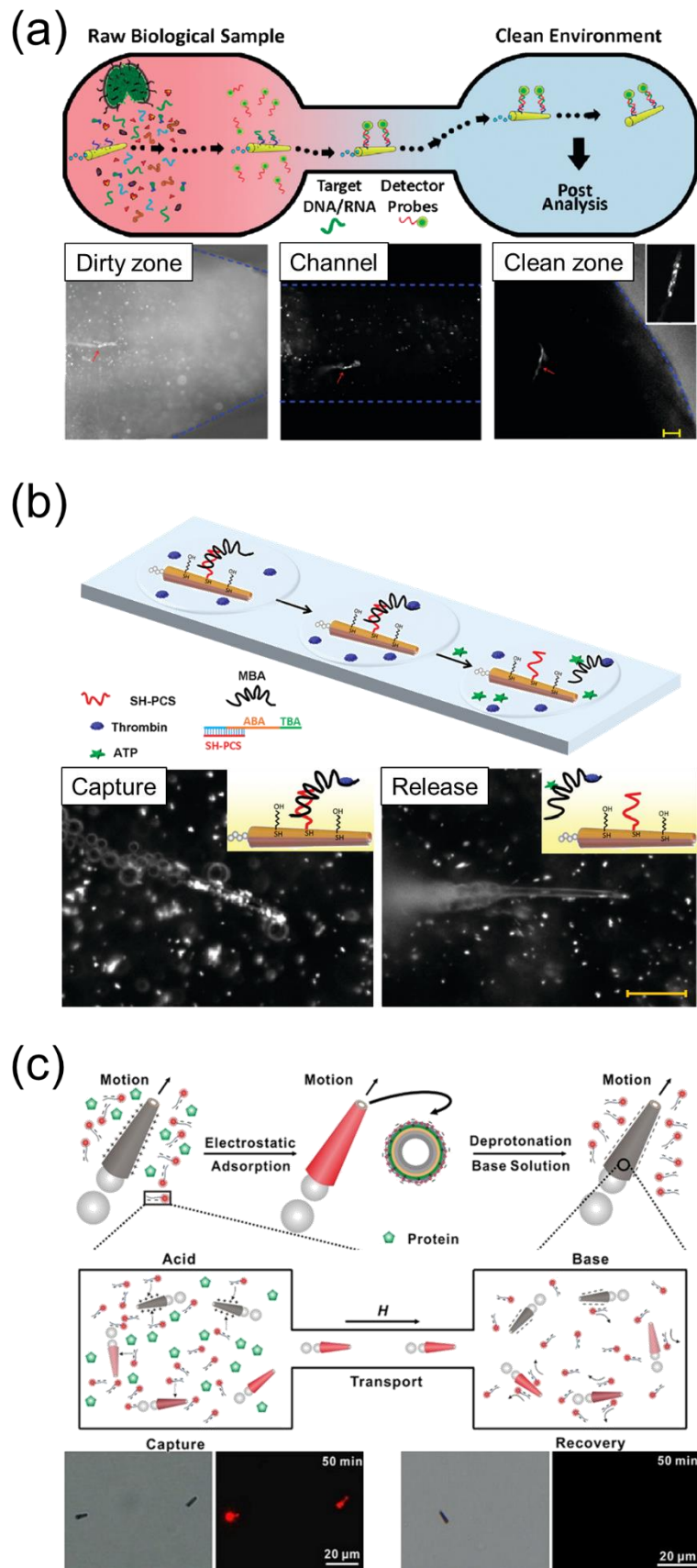
Figure 8. Nucleic acids isolation strategies. (a) Nucleic acids extraction from raw biological samples: optical microscopy images show a bubble-propelled ssDNA probe-modified Au/Pt tubular microrobot which captures a fluorophore-labeled DNA target via

hybridization in a "dirty" zone, transports it across a channel, and reaches a "clean" zone for post-analysis. Scale bar is 60 μm (30 μm for the inset). Adapted with permission from [61]. Copyright 2011 American Chemical Society. (b) Isolation and controlled release of proteins: bubble-propelled Ti/Ni/Au/Pt microrobots are modified with a mixed binding aptamer (MBA) containing both thrombin and ATP aptamers; thrombin is captured by its aptamer, transported by microrobots, and released in an ATP solution. Optical microscopy images demonstrate the release of the target protein after 20 min incubation in the absence (left) or presence (right) of 0.01 M ATP. Scale bar is 30 μm. Adapted with permission from [62]. Copyright 2011 American Chemical Society. (c) Nucleic acids extraction by surface charge-reversible microrobots: bubble-propelled magnetic field-navigable PEI/Ni/Pt tubular microrobots capture FITC-labeled negatively charged nucleic acids in acidic solutions (pH 4) due to their positive surface charge, and release them in basic solutions (pH 11) due to their negative surface charge. Optical and fluorescence microscopy images prove nucleic acids capture by microrobots (50 min in acidic solution) and release (50 min in basic solution). Adapted with permission from [64]. Copyright 2019 Wiley.

4.3. Gene therapy

Gene therapy is a medical treatment based on the delivery of DNA to defective cells to treat or cure a disease or cancer. Lipoplexes, complexes of cationic lipids and anionic DNA linked by ionic interactions, are considered excellent vectors for DNA delivery. They can easily fuse with the cell membrane or be incorporated through endocytosis. Inspired by natural bacteria flagella, lipoplexes-functionalized artificial bacterial flagella have been designed and operated as magnetic microrobots for targeted and single-cell gene therapy (Figure 9(a)).[65] Polymeric helical structures (5 μm in diameter, 16 μm in length) were produced by 3D laser direct writing and covered by thin Ni and Ti layers through electron beam evaporation. The Ni core provided the magnetic property required for microrobots navigation based on the mechanism illustrated in Figure 2(e). At the same time, the Ti layer passivated Ni surface, improved microrobots biocompatibility, and ensured the facile loading of lipoplexes after oxidation to TiO_2. A rotating magnetic field allowed controlling microrobots movement toward targeted cells at speed values as high as ~44 μm s^{-1} for a ~30 Hz frequency and 5 mT magnetic field. When employed for *in vitro* HEK 293 cells transfection studies, they showed efficient delivery of the plasmid DNA in the lipoplexes to the cells in their proximity. In fact, the transfected cells expressed the Venus protein, whose fluorescence has been recorded. Notably, it has been observed that microrobots could transfect cells without influencing cell division or causing cell death, which is highly desired for *in vivo* applications.

Micro/nanorobots are also promising for small interfering RNA (siRNA) therapy. This involves the delivery of gene silencing complexes which cause the suppression of mRNA target sequences, inhibiting the expression of unwanted proteins within the cell. A nanorobot-based approach with greatly enhanced intracellular gene delivery and silencing efficiency compared to conventional methods has been demonstrated (Figure 9(b)).[66] Au nanowires (200 nm in diameter, ~4 μm in length) were prepared by membrane template-assisted electrodeposition and successively modified with Green Fluorescence Protein targeted siRNA (siGFP)

25

hybridized to circular DNA structures obtained via Rolling Circle Amplification (RCA). The small size and motion of GFP/RCA-Au nanorobots under an ultrasound field (6 V, 2.66 MHz) allowed their rapid internalization inside the cell. Nanorobots gene silencing ability has been tested in various cell lines, including HEK 293 cells, which were selected as they easily express recombinant proteins like the GFP. Fluorescence signals were recorded after treatments with nanorobots for different incubation times and GFP/RCA loadings with (dynamic) and without (static) applied ultrasound. The fluorescence of samples treated with static nanorobots was almost unchanged compared to the evident decrease observed for dynamic ones, attributed to their spinning movement inside the cells. Cell viability measurements excluded the possibility that GFP silencing was due to cell death caused by nanorobots. In principle, RCA can support multiple siRNA sequences at once, leading to the simultaneous delivery of several siRNA sequences associated with various diseases or cancers.

Acoustically propelled Au nanorobots were employed as well for the intracellular delivery of sgRNA/Cas9 complex, causing the GFP knockout in B16F10 cells with a ~80% efficiency for dynamic nanorobots and ~30% for static ones within 2 h incubation.[67]
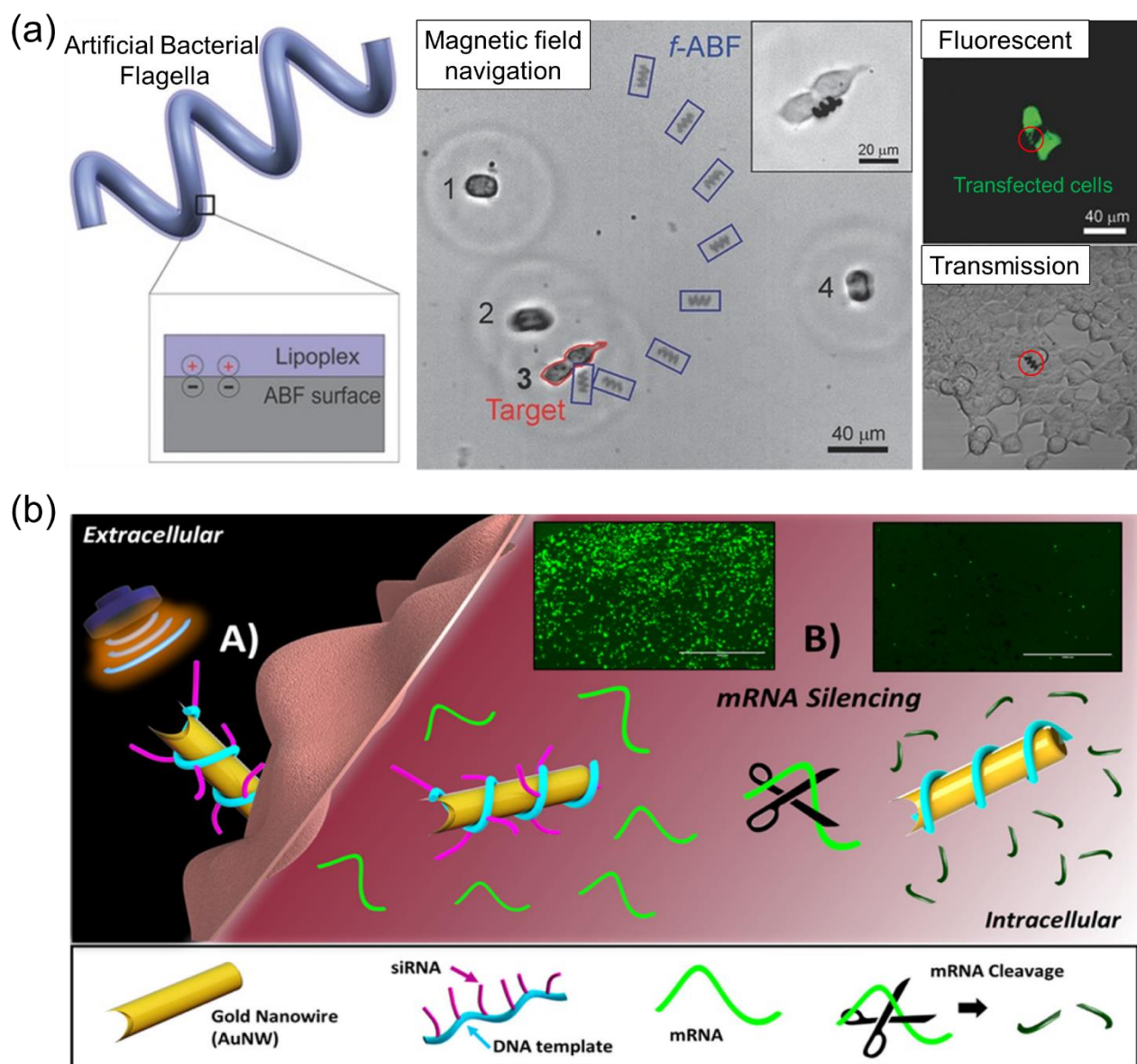
Figure 9. DNA-modified micro/nanorobots for gene therapy. (a) Lipoplexes-functionalized artificial bacteria flagella for targeted gene delivery: time-lapse optical microscopy image shows the precise navigation of a helical microrobot (blue square) toward a targeted HEK 293 cell n. 3 (undergoing division) under a rotating magnetic field (5 mT, 30 Hz) (the time interval of each microrobot's movement is 4 s). The plasmid DNA in lipoplexes successfully transfects cells. Transmission and fluorescent microscopy images demonstrate encoded protein expression in the transfected cells (red circles indicate the microrobot). Adapted with permission from [65]. Copyright 2015 Wiley. (b) Ultrasound-powered nanorobots for intracellular siRNA delivery: the fast internalization and rapid movement of Au nanowires inside HEK 293-GFP cells accelerate mRNA gene silencing. Fluorescence images demonstrate GFP fluorescence decrease after 5 min treatment with nanorobots under ultrasound (6 V, 2.66 MHz) and overnight incubation. Scale bars are 1 mm. Reproduced with permission from [66]. Copyright 2016 American Chemical Society.

4.4. Water remediation

The rapid pace of industrialization and diverse human activities make various harmful pollutants, including heavy metal ions, nano/microplastics, hazardous chemicals, and pathogens, drain the environment. Mercury is one of the most toxic contaminants in water bodies for wildlife and humans. DNA-functionalized microrobots have been proposed as efficient machines for water purification from mercury.[68] These comprised Au/Pt

tubular microrobots prepared by membrane template-assisted electrodeposition (2.5-3 μm in diameter, ~10 μm in length). The Au outer layer ensured a large surface area for immobilizing a thiolated DNA sequence with thymine-thymine (T-T) mismatched base pairs. The mercury sequestration strategy was based on Hg(II) ions property to selectively mediate the generation of T-Hg(II)-T complexes. In fact, Hg(II) binds to N3 of thymidine by replacing the imino proton and cross-links two thymidines to form the T-Hg(II)-T base pair. The microrobots showed a high speed of ~180 μm s^{-1} in the presence of 3% H_2O_2. Aqueous solutions containing 3 ppm Hg(II) ions were exposed for 20 min to microrobots in static and dynamic conditions. The solutions were subsequently analyzed by inductively coupled plasma-mass spectrometry (ICP-MS) to evaluate the residual content of Hg(II). The higher removal efficiency was found for the dynamic microrobots (26%) compared to the static ones (17%), attributed to the DNA-induced "on-the-fly" trapping of Hg(II). This result is particularly remarkable considering the low number of microrobots involved in the experiments (~3000 mL^{-1}). Furthermore, the proposed strategy can also be employed for mercury sensing at trace level, which is essential as well as its successive remediation.

5. Conclusions and future perspectives

In this review, we presented the recent advances in the development and application of DNA-modified micro/nanorobots. First, the most reported mechanisms to power these systems have been described, including catalytic, acoustic, and magnetic actuation. Then, new DNA-based propulsion concepts have been illustrated. These comprise the utilization of DNA as a substrate for the chemotactic movement of enzymatic nanorobots toward apoptotic tumor cells, which is promising for drug delivery and, so, cancer therapy. Nucleospheres, i.e., self-assembled DNA microspheres, are fascinating platforms for the formulation of microrobots due to their easy functionalizability through the DNA chemistry. Moreover, the inclusion of DNA nanodevices in the material's design, such as the pH-responsive DNA nanoswitches, represents a step forward for micro/nanorobots intelligentization, which is one of the big challenges in this research field.

The high specificity of DNA base-pairing combined with the motion dimension has opened new possibilities in various applications. For example, the concept of motion-based sensing has been extended to DNA and RNA. Several approaches have been conceived to transduce the probe-target recognition event into a detectable variation of micro/nanorobots speed, ranging from proof-of-concept reports to compact cellphone-

based sensors with a high market value. Most of the studies involved catalytic microrobots fueled by H_2O_2, whose toxicity was not a problem in those specific cases. We also expect the future investigation of magnetic propulsion for motion-based sensing, taking inspiration from the work of Nguyen and Minteer, who presented the "signal-on" DNA detection as a result of the DNA target-induced hybridization between DNA-modified tubular microrobots and Pt nanoparticles.[42] In particular, we propose to replace the Pt nanoparticles with superparamagnetic beads which, once anchored to the microrobot, will unlock its magnetic motion. Then, magnetic actuation could provide more sensitive DNA detection than bubble-propulsion due to more parameters, such as magnetic field intensity and frequency, which can be precisely tuned.

Furthermore, the fast and efficient fluorescence detection of various cancer biomarkers has been proved. The mechanism involved the fluorescence quenching of a dye-labeled ssDNA probe on micro/nanorobots surface, followed by the fluorescence recovery due to its hybridization with the target. In addition, dual motion and fluorescent-based signaling has been reported. In these works, acoustically powered micro/nanorobots have been preferred, especially when the detection was performed in living cells. Specifically, ultrasound-powered nanorobots showed rapid internalization and effective movement inside the cell.

Different approaches for the "on-the-fly" capture, transport, and release of nucleic acids have been proposed, playing on DNA hybridization, DNA aptamer-protein binding, and microrobots reversible surface charge. These pose the basis for the development of an all-in-one microfluidic device for targeted DNA isolation from a chamber where the raw sample is introduced to a clean chamber for post-processing analyses, such as sensing. Such a device would truly represent an important advance compared to conventional methods for DNA detection, avoiding complex and multiple sample preparation and washing steps. For this purpose, the micro/nanorobot's design must comprise at least one or two components for the propulsion (for example, a catalytic engine to accelerate the recognition and a magnetic element for the controlled manipulation throughout the device), a recognition unit, and a sensing unit. Nevertheless, the fabrication of multi-task micro/nanorobots is challenging.[23]

Intracellular gene delivery to promote or suppress the expression of specific proteins has been shown, taking advantage of the safe operation of acoustic and magnetic micro/nanorobots. Notably, the latter were accurately navigated toward the targeted cell, confirming the advantage of magnetic actuation in biomedical applications. It is worth noting that acoustic and magnetic micro/nanorobots usually enter the cells by physical penetration.

Although it has been verified that this process has not caused cell death, less invasive internalization strategies should be explored. By doing so, it must be taken into account for the use of biocompatible and degradable materials in micro/nanorobots design.

Finally, the original utilization of mismatched DNA-modified microrobots for selectively removing Hg(II) from Hg-polluted waters has also been proven.

As the fields of DNA nanotechnology and micro/nanorobotics are progressing rapidly, we believe that novel, exciting directions will emerge soon. In this regard, inspired by the movie "Big Hero 6" showing tiny microbots linking together in any arrangement thanks to a neurocranial transmitter, we foresee the formulation of complex, intelligent, and programmable nanorobotic swarms taking advantage of the high programmability of DNA interactions. Although total control over the assembly has not been achieved yet, the bases have already been laid: DNA-coated colloids have been used to design sophisticated materials at the colloidal scale with tailored surfaces and shapes (Figure 10).[69] This approach allows the formulation of a limitless number of structures. The possibility of introducing external stimuli, such as the temperature, to trigger or influence the assembly/disassembly of these systems further expand their potential.[70] Indeed, DNA-engineered nanorobots can, in principle, possess the encoding information for their self-assembly into self-propelled superstructures performing tasks beyond the single entity's capability.
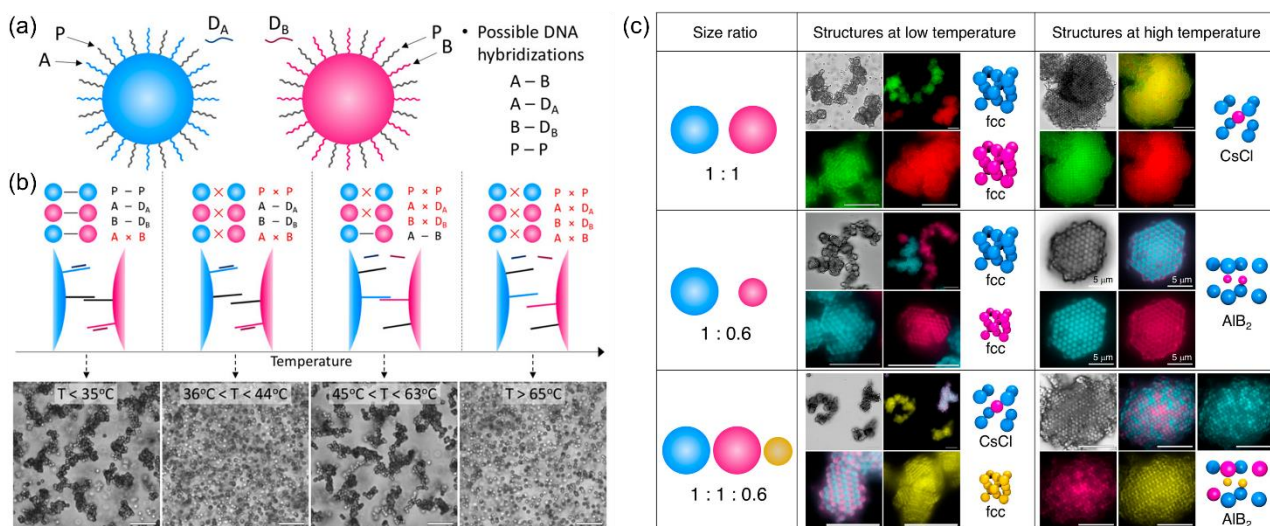

Figure 10. Reconfigurable self-assembly of DNA-coated particles in response to the temperature. (a) Schematic illustration of the reconfigurable self-assembly of two DNA-coated particles of the same size at different temperatures. The blue and red particles are coated with A and B complementary strands, respectively, and self-complementary P DNA strands. DA and DB are displacement strands for A and B DNA strands, respectively. (b) Schematic illustration of specific interactions between DNA-coated particles and the available DNA−DNA bonds, and the corresponding optical images of the DNA-coated particles at different temperatures. (c) DNA-coated particles of various size ratios are programmed to self-assemble into separate crystals at the lower temperature and a single,

different crystal at the higher temperature. Scale bars are 10 μm. Adapted with permission from [70]. Copyright 2020 American Chemical Society.

Acknowledgments

References

(1)   Lu, C. H.; Willner, B.; Willner, I. DNA Nanotechnology: From Sensing and DNA Machines to Drug-Delivery Systems. *ACS Nano* **2013**, *7* (10), 8320–8332. https://doi.org/10.1021/nn404613v.

(2)   Seeman, N. C. DNA in a Material World. *Nature* **2003**, *421* (6921), 427–431. https://doi.org/10.1038/nature01406.

(3)   Chen, Y. J.; Groves, B.; Muscat, R. A.; Seelig, G. DNA Nanotechnology from the Test Tube to the Cell. *Nat. Nanotechnol.* **2015**, *10* (9), 748–760. https://doi.org/10.1038/nnano.2015.195.

(4)   Seeman, N. C.; Sleiman, H. F. DNA Nanotechnology. *Nat. Rev. Mater.* **2018**, *3*, 17068. https://doi.org/10.1038/natrevmats.2017.68.

(5)   Madsen, M.; Gothelf, K. V. Chemistries for DNA Nanotechnology. *Chem. Rev.* **2019**, *119* (10), 6384–6458. https://doi.org/10.1021/acs.chemrev.8b00570.

(6)   Zhao, Y.; Dai, X.; Wang, F.; Zhang, X.; Fan, C.; Liu, X. Nanofabrication Based on DNA Nanotechnology. *Nano Today* **2019**, *26*, 123–148. https://doi.org/10.1016/j.nantod.2019.03.004.

(7)   Hu, Q.; Li, H.; Wang, L.; Gu, H.; Fan, C. DNA Nanotechnology-Enabled Drug Delivery Systems. *Chem. Rev.* **2019**, *119* (10), 6459–6506. https://doi.org/10.1021/acs.chemrev.7b00663.

(8)   Shen, L.; Wang, P.; Ke, Y. DNA Nanotechnology-Based Biosensors and Therapeutics. *Adv. Healthc. Mater.* **2021**, *10* (15), 2002205. https://doi.org/10.1002/adhm.202002205.

(9)   Novotný, F.; Wang, H.; Pumera, M. Nanorobots: Machines Squeezed between Molecular Motors and Micromotors. *Chem* **2020**, *6* (4), 867–884. https://doi.org/10.1016/j.chempr.2019.12.028.

(10)   Soto, F.; Karshalev, E.; Zhang, F.; Esteban Fernandez De Avila, B.; Nourhani, A.; Wang, J. Smart Materials for Microrobots. *Chem. Rev.* **2021**. https://doi.org/10.1021/acs.chemrev.0c00999.

(11)   Wang, B.; Kostarelos, K.; Nelson, B. J.; Zhang, L. Trends in Micro-/Nanorobotics: Materials Development, Actuation, Localization, and System Integration for Biomedical Applications. *Adv. Mater.* **2021**, *33* (4), 2002047. https://doi.org/10.1002/adma.202002047.

(12)   Yu, S.; Cai, Y.; Wu, Z.; He, Q. Recent Progress on Motion Control of Swimming Micro/Nanorobots. *View* **2021**, *2* (5), 20200113. https://doi.org/10.1002/viw.20200113.

(13)   Xu, K.; Liu, B. Recent Progress in Actuation Technologies of Micro/Nanorobots. *Beilstein J. Nanotechnol.* **2021**, *12*, 756–765. https://doi.org/10.3762/bjnano.12.59.

(14)   Ye, H.; Wang, Y.; Xu, D.; Liu, X.; Liu, S.; Ma, X. Design and Fabrication of Micro/Nano-Motors for Environmental and Sensing Applications. *Appl. Mater. Today* **2021**, *23*, 101007. https://doi.org/10.1016/j.apmt.2021.101007.

(15)   Hu, Y.; Liu, W.; Sun, Y. Self-Propelled Micro-/Nanomotors as "On-the-Move" Platforms: Cleaners, Sensors, and Reactors. *Adv. Funct. Mater.* **2021**, 2109181. https://doi.org/10.1002/adfm.202109181.

(16)   Schmidt, C. K.; Medina-Sánchez, M.; Edmondson, R. J.; Schmidt, O. G. Engineering Microrobots for Targeted Cancer Therapies from a Medical Perspective. *Nat. Commun.* **2020**, *11* (1), 5618. https://doi.org/10.1038/s41467-020-19322-7.

(17)   Wu, Z.; Chen, Y.; Mukasa, D.; Pak, O. S.; Gao, W. Medical Micro/Nanorobots in Complex Media. *Chem. Soc. Rev.* **2020**, *49* (22), 8088–8112. https://doi.org/10.1039/d0cs00309c.

(18)   Bazrafshan, A.; Kyriazi, M. E.; Holt, B. A.; Deng, W.; Piranej, S.; Su, H.; Hu, Y.; El-Sagheer, A. H.; Brown, T.; Kwong, G. A.; Kanaras, A. G.; Salaita, K. DNA Gold Nanoparticle Motors Demonstrate Processive Motion with Bursts of Speed up to 50 Nm per Second. *ACS Nano* **2021**, *15* (5), 8427–8438. https://doi.org/10.1021/acsnano.0c10658.

(19)   Ramezani, H.; Dietz, H. Building Machines with DNA Molecules. *Nat. Rev. Genet.* **2020**, *21*, 5–26. https://doi.org/10.1038/s41576-019-0175-6.

(20)   Urso, M.; Ussia, M.; Pumera, M. Breaking Polymer Chains with Self-Propelled Light-Controlled Navigable Hematite Microrobots. *Adv. Funct. Mater.* **2021**, *31* (28), 2101510. https://doi.org/10.1002/adfm.202101510.

(21)   Ussia, M.; Urso, M.; Dolezelikova, K.; Michalkova, H.; Adam, V.; Pumera, M. Active Light-Powered Antibiofilm ZnO Micromotors with Chemically Programmable Properties. *Adv. Funct. Mater.* **2021**,

31 (27), 2101178. https://doi.org/10.1002/adfm.202101178.

(22) Peng, X.; Urso, M.; Pumera, M. Photo-Fenton Degradation of Nitroaromatic Explosives by Light-Powered Hematite Microrobots: When Higher Speed Is Not What We Go For. *Small Methods* **2021**, *5* (10), 2100617. https://doi.org/10.1002/smtd.202100617.

(23) Wang, J. Will Future Microbots Be Task-Specific Customized Machines or Multi-Purpose "All in One" Vehicles? *Nat. Commun.* **2021**, *12*, 7125. https://doi.org/10.1038/s41467-021-26675-0.

(24) Wang, L.; Meng, Z.; Chen, Y.; Zheng, Y. Engineering Magnetic Micro/Nanorobots for Versatile Biomedical Applications. *Adv. Intell. Syst.* **2021**, *3* (7), 2000267. https://doi.org/10.1002/aisy.202000267.

(25) Urso, M.; Iffelsberger, C.; Mayorga-Martinez, C. C.; Pumera, M. Nickel Sulfide Microrockets as Self-Propelled Energy Storage Devices to Power Electronic Circuits "On-Demand." *Small Methods* **2021**, *5* (10), 2100511. https://doi.org/10.1002/smtd.202100511.

(26) Solovev, A. A.; Mei, Y.; Ureña, E. B.; Huang, G.; Schmidt, O. G. Catalytic Microtubular Jet Engines Self-Propelled by Accumulated Gas Bubbles. *Small* **2009**, *5* (14), 1688–1692. https://doi.org/10.1002/smll.200900021.

(27) Li, J.; Rozen, I.; Wang, J. Rocket Science at the Nanoscale. *ACS Nano* **2016**, *10* (6), 5619–5634. https://doi.org/10.1021/acsnano.6b02518.

(28) Paxton, W. F.; Baker, P. T.; Kline, T. R.; Wang, Y.; Mallouk, T. E.; Sen, A. Catalytically Induced Electrokinetics for Motors and Micropumps. *J. Am. Chem. Soc.* **2006**, *128* (46), 14881–14888. https://doi.org/10.1021/ja0643164.

(29) Wang, J.; Gao, W. Nano/Microscale Motors: Biomedical Opportunities and Challenges. *ACS Nano* **2012**, *6* (7), 5745–5751. https://doi.org/10.1021/nn3028997.

(30) Hermanová, S.; Pumera, M. Biocatalytic Micro- and Nanomotors. *Chem. - A Eur. J.* **2020**, *26* (49), 11085–11092. https://doi.org/10.1002/chem.202001244.

(31) Yuan, H.; Liu, X.; Wang, L.; Ma, X. Fundamentals and Applications of Enzyme Powered Micro/Nano-Motors. *Bioact. Mater.* **2021**, *6* (6), 1727–1749. https://doi.org/10.1016/j.bioactmat.2020.11.022.

(32) Hortelao, A. C.; Simó, C.; Guix, M.; Guallar-Garrido, S.; Julián, E.; Vilela, D.; Rejc, L.; Ramos-Cabrer, P.; Cossío, U.; Gómez-Vallejo, V.; Patiño, T.; Llop, J.; Sánchez, S. Swarming Behavior and in Vivo

Monitoring of Enzymatic Nanomotors within the Bladder. *Sci. Robot.* **2021**, *6* (52). https://doi.org/10.1126/SCIROBOTICS.ABD2823.

(33) Venugopalan, P. L.; Esteban-Fernández De Ávila, B.; Pal, M.; Ghosh, A.; Wang, J. Fantastic Voyage of Nanomotors into the Cell. *ACS Nano* **2020**, *14* (8), 9423–9439. https://doi.org/10.1021/acsnano.0c05217.

(34) Xu, L.; Gong, D.; Chen, K.; Cai, J.; Zhang, W. Acoustic Levitation Applied for Reducing Undesired Lateral Drift of Magnetic Helical Microrobots. *J. Appl. Phys.* **2020**, *128*, 184703. https://doi.org/10.1063/5.0026728.

(35) Fernández-Medina, M.; Ramos-Docampo, M. A.; Hovorka, O.; Salgueiriño, V.; Städler, B. Recent Advances in Nano- and Micromotors. *Adv. Funct. Mater.* **2020**, *30* (12), 1908283. https://doi.org/10.1002/adfm.201908283.

(36) Ye, Y.; Tong, F.; Wang, S.; Jiang, J.; Gao, J.; Liu, L.; Liu, K.; Wang, F.; Wang, Z.; Ou, J.; Chen, B.; Wilson, D. A.; Tu, Y.; Peng, F. Apoptotic Tumor DNA Activated Nanomotor Chemotaxis. *Nano Lett.* **2021**, *21* (19), 8086–8094. https://doi.org/10.1021/acs.nanolett.1c02441.

(37) Inaba, H.; Hatta, K.; Matsuura, K. Directional Propulsion of DNA Microspheres Based on Light-Induced Asymmetric Growth of Peptide Nanofibers. *ACS Appl. Bio Mater.* **2021**, *4* (7), 5425–5434. https://doi.org/10.1021/acsabm.1c00146.

(38) Patino, T.; Porchetta, A.; Jannasch, A.; Lladó, A.; Stumpp, T.; Schäffer, E.; Ricci, F.; Sánchez, S. Self-Sensing Enzyme-Powered Micromotors Equipped with PH-Responsive DNA Nanoswitches. *Nano Lett.* **2019**, *19* (6), 3440–3447. https://doi.org/10.1021/acs.nanolett.8b04794.

(39) Urso, M.; Tumino, S.; Bruno, E.; Bordonaro, S.; Marletta, D.; Loria, G. R.; Avni, A.; Shacham-Diamand, Y.; Priolo, F.; Mirabella, S. Ultrasensitive Electrochemical Impedance Detection of Mycoplasma Agalactiae DNA by Low-Cost and Disposable Au-Decorated NiO Nanowall Electrodes. *ACS Appl. Mater. Interfaces* **2020**, *12* (44), 50143–50151. https://doi.org/10.1021/acsami.0c14679.

(40) Kagan, D.; Calvo-Marzal, P.; Balasubramanian, S.; Sattayasamitsathit, S.; Manesh, K. M.; Flechsig, G. U.; Wang, J. Chemical Sensing Based on Catalytic Nanomotors: Motion-Based Detection of Trace Silver. *J. Am. Chem. Soc.* **2009**, *131* (34), 12082–12083. https://doi.org/10.1021/ja905142q.

(41) Wu, J.; Balasubramanian, S.; Kagan, D.; Manesh, K. M.; Campuzano, S.; Wang, J. Motion-Based DNA

Detection Using Catalytic Nanomotors. *Nat. Commun.* **2010**, *1*, 36. https://doi.org/10.1038/ncomms1035.

(42) Van Nguyen, K.; Minteer, S. D. DNA-Functionalized Pt Nanoparticles as Catalysts for Chemically Powered Micromotors: Toward Signal-on Motion-Based DNA Biosensor. *Chem. Commun.* **2015**, *51* (23), 4782–4784. https://doi.org/10.1039/c4cc10250a.

(43) Xie, Y.; Fu, S.; Wu, J.; Lei, J.; Ju, H. Motor-Based Microprobe Powered by Bio-Assembled Catalase for Motion Detection of DNA. *Biosens. Bioelectron.* **2017**, *87*, 31–37. https://doi.org/10.1016/j.bios.2016.07.104.

(44) Fu, S.; Zhang, X.; Xie, Y.; Wu, J.; Ju, H. An Efficient Enzyme-Powered Micromotor Device Fabricated by Cyclic Alternate Hybridization Assembly for DNA Detection. *Nanoscale* **2017**, *9* (26), 9026–9033. https://doi.org/10.1039/c7nr01168g.

(45) Zhang, X.; Chen, C.; Wu, J.; Ju, H. Bubble-Propelled Jellyfish-like Micromotors for DNA Sensing. *ACS Appl. Mater. Interfaces* **2019**, *11* (14), 13581–13588. https://doi.org/10.1021/acsami.9b00605.

(46) Draz, M. S.; Kochehbyoki, K. M.; Vasan, A.; Battalapalli, D.; Sreeram, A.; Kanakasabapathy, M. K.; Kallakuri, S.; Tsibris, A.; Kuritzkes, D. R.; Shafiee, H. DNA Engineered Micromotors Powered by Metal Nanoparticles for Motion Based Cellphone Diagnostics. *Nat. Commun.* **2018**, *9*, 4282. https://doi.org/10.1038/s41467-018-06727-8.

(47) Fang, Y.; Zhang, L.; Li, Z.; Li, Y.; Huang, C.; Lu, X. *MicroRNAs in DNA Damage Response, Carcinogenesis, and Chemoresistance*, 1st ed.; Elsevier Inc., 2017; Vol. 333. https://doi.org/10.1016/bs.ircmb.2017.03.001.

(48) Esteban-Fernández De Ávila, B.; Martín, A.; Soto, F.; Lopez-Ramirez, M. A.; Campuzano, S.; Vásquez-Machado, G. M.; Gao, W.; Zhang, L.; Wang, J. Single Cell Real-Time MiRNAs Sensing Based on Nanomotors. *ACS Nano* **2015**, *9* (7), 6756–6764. https://doi.org/10.1021/acsnano.5b02807.

(49) Qualliotine, J. R.; Bolat, G.; Beltrán-Gastélum, M.; de Ávila, B. E. F.; Wang, J.; Califano, J. A. Acoustic Nanomotors for Detection of Human Papillomavirus–Associated Head and Neck Cancer. *Otolaryngol. - Head Neck Surg.* **2019**, *161* (5), 814–822. https://doi.org/10.1177/0194599819866407.

(50) Beltrán-Gastélum, M.; Esteban-Fernández de Ávila, B.; Gong, H.; Venugopalan, P. L.; Hianik, T.; Wang, J.; Subjakova, V. Rapid Detection of AIB1 in Breast Cancer Cells Based on Aptamer-

Functionalized Nanomotors. *ChemPhysChem* **2019**, *20* (23), 3177–3180. https://doi.org/10.1002/cphc.201900844.

(51)   Báez, D. F.; Ramos, G.; Corvalán, A.; Cordero, M. L.; Bollo, S.; Kogan, M. J. Effects of Preparation on Catalytic, Magnetic and Hybrid Micromotors on Their Functional Features and Application in Gastric Cancer Biomarker Detection. *Sensors Actuators, B Chem.* **2020**, *310*, 127843. https://doi.org/10.1016/j.snb.2020.127843.

(52)   Esteban-Fernández De Ávila, B.; Lopez-Ramirez, M. A.; Báez, D. F.; Jodra, A.; Singh, V. V.; Kaufmann, K.; Wang, J. Aptamer-Modified Graphene-Based Catalytic Micromotors: Off-On Fluorescent Detection of Ricin. *ACS Sensors* **2016**, *1* (3), 217–221. https://doi.org/10.1021/acssensors.5b00300.

(53)   Molinero-Fernández, Á.; Moreno-Guzmán, M.; López, M. Á.; Escarpa, A. Biosensing Strategy for Simultaneous and Accurate Quantitative Analysis of Mycotoxins in Food Samples Using Unmodified Graphene Micromotors. *Anal. Chem.* **2017**, *89* (20), 10850–10857. https://doi.org/10.1021/acs.analchem.7b02440.

(54)   Singh, V. V.; Kaufmann, K.; de Ávila, B. E. F.; Karshalev, E.; Wang, J. Molybdenum Disulfide-Based Tubular Microengines: Toward Biomedical Applications. *Adv. Funct. Mater.* **2016**, *26* (34), 6270–6278. https://doi.org/10.1002/adfm.201602005.

(55)   Zhao, L.; Liu, Y.; Xie, S.; Ran, P.; Wei, J.; Liu, Q.; Li, X. Janus Micromotors for Motion-Capture-Ratiometric Fluorescence Detection of Circulating Tumor Cells. *Chem. Eng. J.* **2020**, *382*, 123041. https://doi.org/10.1016/j.cej.2019.123041.

(56)   Cogal, G. C.; Karaca, G. Y.; Uygun, E.; Kuralay, F.; Oksuz, L.; Remskar, M.; Oksuz, A. U. RF Plasma-Enhanced Conducting Polymer/W5O14 Based Self-Propelled Micromotors for MiRNA Detection. *Anal. Chim. Acta* **2020**, *1138*, 69–78. https://doi.org/10.1016/j.aca.2020.07.010.

(57)   Yurdabak Karaca, G.; Kuralay, F.; Bingol Ozakpinar, O.; Uygun, E.; Koc, U.; Ulusoy, S.; Bosgelmez Tinaz, G.; Oksuz, L.; Uygun Oksuz, A. Catalytic Au/PEDOT/Pt Micromotors for Cancer Biomarker Detection and Potential Breast Cancer Treatment. *Appl. Nanosci.* **2021**. https://doi.org/10.1007/s13204-021-01735-5.

(58)   Celik Cogal, G.; Das, P. K.; Yurdabak Karaca, G.; Bhethanabotla, V. R.; Uygun Oksuz, A.

Fluorescence Detection of MiRNA-21 Using Au/Pt Bimetallic Tubular Micromotors Driven by Chemical and Surface Acoustic Wave Forces. *ACS Appl. Bio Mater.* **2021**, *4* (11), 7932–7941. https://doi.org/10.1021/acsabm.1c00854.

(59) Karaca, G. Y.; Kuralay, F.; Uygun, E.; Ozaltin, K.; Demirbuken, S. E.; Garipcan, B.; Oksuz, L.; Oksuz, A. U. Gold-Nickel Nanowires as Nanomotors for Cancer Marker Biodetection and Chemotherapeutic Drug Delivery. *ACS Appl. Nano Mater.* **2021**, *4* (4), 3377–3388. https://doi.org/10.1021/acsanm.0c03145.

(60) Park, S.; Yossifon, G. Micromotor-Based Biosensing Using Directed Transport of Functionalized Beads. *ACS sensors* **2020**, *5* (4), 936–942. https://doi.org/10.1021/acssensors.9b02041.

(61) Kagan, D.; Campuzano, S.; Balasubramanian, S.; Kuralay, F.; Flechsig, G. U.; Wang, J. Functionalized Micromachines for Selective and Rapid Isolation of Nucleic Acid Targets from Complex Samples. *Nano Lett.* **2011**, *11* (5), 2083–2087. https://doi.org/10.1021/nl2005687.

(62) Orozco, J.; Campuzano, S.; Kagan, D.; Zhou, M.; Gao, W.; Wang, J. Dynamic Isolation and Unloading of Target Proteins by Aptamer-Modified Microtransporters. *Anal. Chem.* **2011**, *83* (20), 7962–7969. https://doi.org/10.1021/ac202029k.

(63) Amouzadeh Tabrizi, M.; Shamsipur, M.; Saber, R.; Sarkar, S. Isolation of HL-60 Cancer Cells from the Human Serum Sample Using MnO2-PEI/Ni/Au/Aptamer as a Novel Nanomotor and Electrochemical Determination of Thereof by Aptamer/Gold Nanoparticles-Poly(3,4-Ethylene Dioxythiophene) Modified GC Electrode. *Biosens. Bioelectron.* **2018**, *110*, 141–146. https://doi.org/10.1016/j.bios.2018.03.034.

(64) Luo, M.; Jiang, Y.; Su, J.; Deng, Z.; Mou, F.; Xu, L.; Guan, J. Surface Charge-Reversible Tubular Micromotors for Extraction of Nucleic Acids in Microsystems. *Chem. - An Asian J.* **2019**, *14* (14), 2503–2511. https://doi.org/10.1002/asia.201900427.

(65) Qiu, F.; Fujita, S.; Mhanna, R.; Zhang, L.; Simona, B. R.; Nelson, B. J. Magnetic Helical Microswimmers Functionalized with Lipoplexes for Targeted Gene Delivery. *Adv. Funct. Mater.* **2015**, *25* (11), 1666–1671. https://doi.org/10.1002/adfm.201403891.

(66) Esteban-Fernández De Ávila, B.; Angell, C.; Soto, F.; Lopez-Ramirez, M. A.; Báez, D. F.; Xie, S.; Wang, J.; Chen, Y. Acoustically Propelled Nanomotors for Intracellular SiRNA Delivery. *ACS Nano*

2016, *10* (5), 4997–5005. https://doi.org/10.1021/acsnano.6b01415.

(67)   Hansen-Bruhn, M.; de Ávila, B. E. F.; Beltrán-Gastélum, M.; Zhao, J.; Ramírez-Herrera, D. E.; Angsantikul, P.; Vesterager Gothelf, K.; Zhang, L.; Wang, J. Active Intracellular Delivery of a Cas9/SgRNA Complex Using Ultrasound-Propelled Nanomotors. *Angew. Chemie - Int. Ed.* **2018**, *57* (10), 2657–2661. https://doi.org/10.1002/anie.201713082.

(68)   Wang, H.; Khezri, B.; Pumera, M. Catalytic DNA-Functionalized Self-Propelled Micromachines for Environmental Remediation. *Chem* **2016**, *1* (3), 473–481. https://doi.org/10.1016/j.chempr.2016.08.009.

(69)   Rogers, W. B.; Shih, W. M.; Manoharan, V. N. Using DNA to Program the Self-Assembly of Colloidal Nanoparticles and Microparticles. *Nat. Rev. Mater.* **2016**, *1*, 16008. https://doi.org/10.1038/natrevmats.2016.8.

(70)   Oh, J. S.; Yi, G. R.; Pine, D. J. Reconfigurable Self-Assembly and Kinetic Control of Multiprogrammed DNA-Coated Particles. *ACS Nano* **2020**, *14* (4), 4595–4600. https://doi.org/10.1021/acsnano.0c00164.